International Journal of Pharmaceutics 548 (2018) 1–14

Contents lists available at ScienceDirect

International Journal of Pharmaceutics

journal homepage: www.elsevier.com/locate/ijpharm

Spherical neutral gold nanoparticles improve anti-inflammatory response, oxidative stress and fibrosis in alcohol-methamphetamine-induced liver injury in rats

Thaís Gomes de Carvalho[a,c], Vinícius Barreto Garcia[a,c], Aurigena Antunes de Araújo[d], Luiz Henrique da Silva Gasparotto[e], Heloiza Silva[e], Gerlane Coelho Bernardo Guerra[d], Emilio de Castro Miguel[f], Renata Ferreira de Carvalho Leitão[g], Deiziane Viana da Silva Costa[g], Luis J Cruz[h], Alan B. Chan[i], Raimundo Fernandes de Araújo Júnior[a,b,c,*]

[a] Department of Morphology, Federal University of Rio Grande do Norte, Natal 59072-970, RN, Brazil
[b] Post-Graduation Programme in Structural and Functional Biology, Federal University of Rio Grande do Norte, Natal 59072-970, RN, Brazil
[c] Post-Graduation Programme in Health Science, Federal University of Rio Grande do Norte, Natal 59072-970, RN, Brazil
[d] Department of Biophysics and Pharmacology, Post-Graduation Programme in Public Health, Post-graduation Programme in Pharmaceutical Science, Federal University of Rio Grande do Norte, Natal 59072-970, RN, Brazil
[e] Group of Biological Chemistry and Chemometrics, Institute of Chemistry, Federal University of Rio Grande do Norte, Natal 59072-970, RN, Brazil
[f] Department of Physical/Analytical Center/UFC, Fortaleza, CE, Brazil
[g] Department of Morphology/Post-graduate Program in Morphology/UFC, Fortaleza, CE, Brazil
[h] TranslationalNanobiomaterials and Imaging, Department of Radiology, Leiden University Medical Center, 2333 ZA Leiden, The Netherlands
[i] Percuros B.V, 2333 CL Leiden, The Netherlands

ARTICLE INFO

Keywords:
Gold nanoparticles
Ethanol
Methamphetamine
Toxicity and Kupffer cells

ABSTRACT

This study aimed to elucidate the anti-inflammatory, anti-oxidant and antifibrotic effects of gold nanoparticles (GNPs) in rats subjected to liver injury with ethanol and Methamphetamine (METH). The liver injury was induced by gavage administrations of 30% alcoholic solution (7 g/kg) once a day during 28 days, followed by METH (10 mg/kg) on the 20th and 28th days of treatment. GNPs treatment (724.96 μg/kg) during the ethanol and METH exposure was associated with reduced steatosis, hepatic cord degeneration, fibrosis and necrosis. Furthermore, there was a reduction in biochemical markers of liver damage and oxidative stress, and pro-inflammatory cytokines IL-1β and TNF-α, compared to ethanol + METH group alone. A decrease of FGF, SOD-1 and GPx-1 expression was also observed. GNPs down-regulated the activity of Kupffer cells and hepatic stellate cells affecting the profile of their pro-inflammatory cytokines, oxidative stress and fibrosis through modulation of signaling pathways AKT/PI3K and MAPK in ethanol + METH-induced liver injury in a rat model.

1. Introduction

Many drugs, including alcohol and stimulants, are used in social contexts, perhaps because they enhance prosocial behaviors such as social bonding, talking, and empathy (Kirkpatrick and De Wit, 2013; Sayette et al., 2012). Poly-substance use is a term coined to denote the concomitant or sequential consumption of more than one psychoactive drug over an interval of at least 12 months for either therapeutic or recreative purposes. Amongst the substances that are co-administered with illicit drugs, ethanol is undoubtedly the most prevalent chemical responsible for the increasing number of hospital admissions and deaths (Winkler et al., 2016). Ethanol is frequently co-used with psychostimulant drugs such as methamphetamine (METH) or cocaine (Kedia et al., 2007) in order to enhance and prolong the drug effects.

Evidence suggests that the co-administration of ethanol and cocaine produces amplified and extended subjective effect (Ikegami et al., 2002), fewer studies have examined the somatic impact of the METH-ethanol combination in brain (Zendulka et al., 2012; Almalki et al., 2018; Wells et al., 2016). Concerning toxic effects on liver, (Koriem and Soliman, 2014) found that a hoop of edema in the periportal area compresses the surrounding hepatocytes, leading to formation of hyperemic vessels. The association of ethanol and METH produces a variety of histological abnormalities in liver such as abundant cytoplasmic lipid droplets diffusely distributed along the lobules. Besides, a

* Corresponding author: Federal University of Rio Grande do Norte, Lagoa Nova, SN, 1524 Natal, Brazil.
E-mail address: araujojr@cb.ufrn.br (R.F. de Araújo Júnior).

https://doi.org/10.1016/j.ijpharm.2018.06.008
Received 16 February 2018; Received in revised form 24 May 2018; Accepted 4 June 2018
Available online 07 June 2018
0378-5173/

pronounced deposition of collagen fibers between the hepatocytes and the endothelial cells of the sinusoids results in an apparent reduction of the size and density of the hepatocytes in the sinusoids and in the bile canaliculi (Pontes et al., 2008).

Three mechanisms have been proposed for alcoholic liver injury: (i) acetaldehyde toxicity (Guo et al., 2009); (ii) metabolic generation of reactive oxygen species (ROS) or exposure to oxidative stress (Tang et al., 2014); and (iii) oxidative stress in hepatocytes caused by immune response (Chen et al., 2011; Park et al., 2013). The latter has been found in alcoholic-liver-injury patients (Chen et al., 2011), which helps prevent ethanol-induced liver disease.

In liver injury, activated Kupffer cells release a number of soluble agents, including cytokines, such as TGF-β, and TNF-α, ROS (Kang et al., 2008) and factor nuclear kappa B (NF-κB) translocates to the nucleus, in which it binds to the promoter of target genes such as TNF-α and other pro-inflammatory cytokines (Son et al., 2011). These factors act on hepatic stellate cell (HSC), which are localized in the para-sinusoidal space (Wen et al., 2013). The activated phosphatidylinositol-4,5-bisphosphate 3-kinase (PI3-K) participate in regulation of HSC migration, proliferation, collagen secretion and adhesion(Friedman, 2000) besides being involved in regulating a number of cellular responses, such as cell growth, survival and migration. The protein kinase B (Akt or PKB) is downstream of PI3-K and activation of Akt is associated with HSC proliferation and α1 (I) collagen transcription and translation (Reif et al., 2003).

Functionalized spherical gold nanoparticles (GNPs) with controlled geometrical and optical properties are the subject of intensive studies and biomedical applications, including genomics, biosensorics, immunoassay (Bartneck et al., 2014; He et al. 2008), clinical chemistry (Bartneck et al., 2014), laser phototherapy of cancer cells (Gunes et al., 2010), the targeted delivery of drugs (Aslan et al., 2004), DNA and antigens (Dykman and Bogatyrev, 2000), optical bioimaging and the monitoring of cells (Hirsch et al., 2003) and tissues with the use of state-of-the-art detection systems.

Investigation of GNPs cytotoxicity focuses on their size, shape, doses and surrounding ligands being those chemically positive and negative charged responsible for causing cell damages through oxidative alterations in mitochondrial membrane potential (De and Vincent, 2008; Schaeublin et al., 2011). Spherical neutral GNPs are more suitable for biomedical application due to the their inability in removing electrons from molecules, such as membrane lipids and mitochondria, as well as generating free radicals (Loumaigne et al., 2010; Fröhlich, 2012). Local macrophages like kupffer cells ingest foreign materials such as pathogens and nanoparticles, and recruit additional macrophages to the inflamed microenvironment, producing cytokines including TNF-α, IL-6 and TGF-β that up-regulate the inflammatory process (Tilg and Alexander, 2008). Positively charged nanoparticles are preferentially taken up by monocyte-derived macrophages and Kupffer cells that have an M2-like phenotype which produce high level of TGF-β (MacParland et al., 2017).

In this context, macrophages like Kupffer cells therefore not only represent attractive targets for nanomedicine in liver disease, but they also need to be considered as potential particle scavenging cells in any kind of parenteral nanoparticle administration. As such, changing local Kupffer cell behavior may affect the progress of inflammation-related disorders. Therefore, the aim of the present work was to evaluate the anti-inflammatory, antioxidant and antifibrotic effect of GNP in an animal model of ethanol and METH-induced liver injury through an analysis of several markers.

2. Methods

2.1. Chemicals

The absolute ethyl alcohol (PA 99.8%) was obtained from Vetec Quimica, Brazil. Methamphetamine (METH) was acquired from Fisher Scientific, according to the law 10.357 of December 27, 2001, which establishes rules for production, control and inspection of chemical substances.

Murine macrophage cells (RAW 264.7; cat. no. TIB-71) were obtained from American Type Culture Collection (Manassas, VA, USA). Dulbecco's modified Eagle's medium (DMEM) was purchased from Invitrogen Corporation (Carlsbad, CA, USA); fetal bovine serum from Hyclone Company (Logan, UT, USA).

Antibodies anti-TGF- β, FGF, SOD-1, GPX, IL-1β, TNF-β and MIF were obtained from Santa Cruz Biotechnology Enterprise, Brazil. Streptavidin-HRP-conjugated secondary antibody (Biocare Medical, Concord, CA, USA), TrekAvidin-HRP Label + Kit (Biocare Medical, Dako, USA), IL-1β, IL-10, TNF-α and ELISA kit (R&D Systems, Minneapolis, MN, USA) were also utilized in this study.

2.2. Cell culture

RAW 264.7 macrophage cells were grown in DMEM medium with 10% fetal bovine serum. Cells were seeded at a density of 5×10^4 cells per well in 6-well plates and reached 50–60% confluence 24-h after seeding, just before exposure to the non-cytotoxic concentration of GNPs in 10 μg/mL for treatment (Zhang et al. 2011). The cells were maintained in a 5% CO^2 incubator at 37 °C and 95% humidified air. Cells were subsequently analysed by a phase-contrast microscope.

2.3. Immunofluorescence

RAW 264.7 macrophage cells were plated onto glass coverslips in 24 well plates (5×10^4 cells/well) and allowed to grow for 24 h. The cells were then washed, fixed with 1% paraformaldehyde, permeabilized with Triton-X and incubated with 100 μL of GNPs and 4′,6-diamidino-2-phenylindole was used for nuclear stainingfor 10 min in a humid atmosphere at room temperature. Control experiments were performed under the same conditions but without GNPs addition. The glass coverslips were then directly observed with the Leica DM5500 B fluorescence microscope (filter settings: TXR, Cy7, FITC and DAPI), equipped with a condenser using laser excitation from 512 to 542 nm.

2.4. Animal

Thirty six Wistar rats male weighing between 270 g and 300 g, obtained from the animal house of Department of Biophysical and Pharmacology – Federal University of Rio Grande do Norte (UFRN), Natal, Brazil, were randomly divided into six groups of six animals each and used for experiments. Animals were housed in cages with free access to food and water at temperature and humidity controlled environment under a 12 h light/dark cycle. Animals were treated according to the ethical principles for animal experimentation. All experiments were approved by UFRN Ethics Committee (approval number: 018/2015).

2.5. Preparation and administration of ethanol

7 g per kg body weight of 30% v/v ethanol solution was used as chronic dose in this experiment and 30 g of absolute ethanol was dissolved in distilled water and made up to 100 ml, then 6.2 ml of the solution was daily administered for 28 days to each rat treated with ethanol (de Araújo et al., 2016).

2.6. Preparation and administration of methamphetamine

We used the dose of 10 mg/kg for METH, in which 25 mg of METH were diluted in 10 ml of distilled water. Each animal received 0.1 ml of this solution, which corresponds to 2.5 mg in each dose (Halpin et al., 2013).

2.7. Production of gold nanoparticles

Gold nanoparticles (GNPs) were obtained from a partnership with the Department of Chemistry of the Federal University of Rio Grande do Norte-UFRN, Brazil. These GNPs are produced as described by (Gasparotto et al., 2012).

First, Au^{3+} was reduced by glycerol in alkaline medium and polyvinylpyrrolidone was used to stabilize the gold nanoparticles. Diluted HCl was then added to bring the solution pH to 7 and generate neutral GNPs. Considering the quantitative transformation of gold ions into nanoparticles, the concentration of GNPs was estimated to be 197 μg/mL^{-1}. The final mixture has a dark-red color due to the GNPs formation of 7.4 ± 1.6 nm in size.

A Zeta-Meter 3.0 + system (Zeta-Meter Inc., USA) at a temperature of 25 ± 2 °C was used to determine the electrophoretic mobility of the GNPs colloidal solution (20 ml). The zeta potential was calculated using the Smoluchowski equation:

$$\zeta = \frac{\mu_E \eta 0}{\varepsilon_0 \varepsilon_r}$$

where μ_E is the electrophoretic mobility, η_0 is the continuous phase viscosity, $\mathcal{E}_0$ is the permittivity of a vacuum, and $_r$ is the relative permeability of the continuous phase.

2.8. Dosage and administration of gold nanoparticles

The doses of GNPs were chosen through a pilot project, the doses of 700 μg/kg, 1000 μg/kg and 1.500 μg/kg were tested. The dose 700 μg/kg showed best results in decreased inflammatory cytokines IL-1β and TNF-α (de Araújo et al., 2017). The dose of 700 μg/kg was used to calculate the doses to be used in the experiment, based on a gold nanoparticle formulation with a concentration of 197 μg/mL^{-1}.

The doses were adjusted so that for all groups treated by the oral route by gavage the final volume used was standardized in 1 ml. In order to evaluate the dose-dependent effect, the doses were fractionated into 3: starting with the highest dose: 724.96 μg/kg (GNP3); an intermediate dose corresponding to 362.48 μg/kg (GNP2); and finally the third dose with the lowest concentration: 181.48 μg/kg (GNP1).

2.9. Induction of ethanol and METH-induced liver injury

The protocol for hepatic injury induction by exposure to alcohol and METH is summarized below:

1) Animals were treated with GNP1, GNP2 and GNP3 one hour before ethanol administration (30%, 7 g/kg) by oral gavage. Each treatment had three doses to be tested: 181.48 μg/kg, 362.48 μg/kg and 724.96 μg/kg, respectively.
2) Saline solution (NaCl 0.9%) was administered by oral gavage once a week every six days during the first and second week of hepatic injury induction. Methamphetamine was administrated by oral gavage on the 3rd and 4th weeks in place of the saline solution. Saline/Methamphetamine were administered by oral gavage 3 h after ethanol. In the non-methamphetamine groups, saline solution was used by oral gavage to simulate the methamphetamine in the 3rd and 4th week.
3) Step 1 was repeated 7 days a week during 28 days.
4) Step 2 was repeated once a week every 7 days until the end of 28 days of injury induction.

Euthanasia was performed on the 29th day by intraperitoneal injection of Ketamine 7.5 ml/kg (50 mg/ml) and Xylazine 2.5 ml/kg (20 mg/ml). All animal groups were fasted for 12 h to perform the subsequent biochemical analysis. Once unconscious, the animals underwent cardiac puncture followed by removal of the liver.

Liver fragments were frozen at −80 °C for cytokine and oxidative stress analysis, Western blot quantification, qPCR and ultra-structural evaluation using the Transmission Electron Microscopy technique. Other liver fragments were immersed in 10% buffered formalin for histopathological Analysis.

3. Biodistribution of gold nanoparticles

3.1. Conjugation of near-infrared (NIR) fluorescence to the GNPs

Firstly, GNPs were conjugated to the thiol group of the alpha-amino-omega-mercapto poly(ethylene glycol) hydrochloride (SH-PEG-NH2, MW 3.000 g/mol) during 3 h at room temperature. The excess of non-conjugated SH-PEG-NH2 was removed by dialysis (for three days in a membrane Spectra/MWCO: 6-8000) against sodium citrate 2.2 mM. The GNPs-PEG-NH2 were coupled to the IRDye® 680RD NHS ester in bicarbonate buffer (pH 8.1) during 12 h at room temperature. The GNPs-PEG-IRDye complex was then purified by dialysis (for four days in a membrane Spectra/MWCO: 6-8000) against sodium citrate 2.2 mM and the solution was changed two times a day.

3.2. Ex vivo fluorescence imaging of major organs and quantification

6 weeks oldfemale BALB/c mice (n = 3–4) (Charles River, France) were sacrificed after 48 h of intravenous injection (I.V) of the GNPs at three different concentrations (GNP1;GNP2 and GNP3). After 48 h, all major organs were excised for *ex vivo* fluorescence imaging. Images were acquired 700 nm at a resolution of 85 mm. The data were analyzed using Pearl Impulse software, version 3.01 (LI-COR Biosciences, Lincoln, NE, USA). Total fluorescence intensity was determined by drawing a region of interest (ROI). The size and shape of the ROI was the same.

3.3. Antioxidant activity of GNPs

The antioxidant effect of GNPs was evaluated through the GSH consumption, MDA formation and MPO inhibition. Liver samples were harvested as described above and stored at −80 °C until required for assay. After homogenisation and centrifugation (2000 × *g* for 20 min), MPO activity was determined by a previously described colorimetric method (De Araújo et al. 2016). Results are reported as units of MPO per gram of tissue.

To quantify the increase in free radicals in the liver sample, MDA content was measured via the assay described by (Esterbauer and Kevin, 1990). Liver samples were suspended in buffer Tris HCl 1:5 (w/v) and minced with scissors for 15 s on an ice-cold plate. The resulting suspension was homogenised for 2 min with an automatic Potter homogenizer and centrifuged at 2500 × *g* at 4 °C for 10 min. The supernatants were assayed to determine MDA content. The results are expressed as nanomoles of MDA per gram of tissue.

GSH levels in the liver tissues were measured to antioxidant. GSH content was measured via the assay described by (de Araújo et al., 2017). Liver samples (5 per group) were stored at 70 °C until use. Liver tissue homogenates (0.25 ml of a 5% tissue solution prepared in 0.02 M EDTA) were added to 320 ml of distilled water and 80 ml of 50% TCA. Samples were centrifuged at 3000 rpm for 15 min at 4 °C. The supernatant (400 ml) was added to 800 ml of 0.4 M Tris buffer at pH 8.9 and 20 μL of 0.01 M DTNB. The absorbance of each sample was measured at 420 nm, and the results were reported as level of GSH per milligram of tissue.

3.4. Cytokine analysis

Liver samples (three samples per group) were stored at −80 °C until use. The tissue was homogenized and processed as described by (Safieh-Garabedian et al., 1995). Levels of IL-1β (detection range: 62.5–4000 pg/mL; sensitivity or lower limit of detection [LLD]:

12.5 ng/mL of recombinant mouse IL-1β), IL-10 (detection range: 62.5–4000 pg/mL; sensitivity or LLD: 12.5 ng/mL of recombinant mouse IL-10) and TNF-α (detection range: 62.5–4000 pg/mL; sensitivity or LLD: 50 ng/mL of recombinant mouse TNF-α) in the intestinal samples were determined with a commercial ELISA kit (R&D Systems, Minneapolis, MN, *USA*), as described previously. All samples were within the wavelength used in UV–VIS spectrophotometry (absorbance measured at 490 nm).

3.5. Histological analysis from hepatic parenchyma

Liver samples were fixed in 10% neutral buffered formalin, dehydrated and embedded in paraffin. Sections of 5 μm thickness were obtained for hematoxylin–eosin staining (H&E) and examined by light microscopy (40×, Nikon E200 LED). Three sections of liver (six animals per group) were analyzed by two pathologists. Liver pathology was scored as follows: steatosis (the percentage of liver cells containing fat): < 25% = 1, 25–50% = 2, 50–75% = 3, > 75% = 4.; inflammation and necrosis: 1 focus per low-power field; 2 or more foci. Pathology was scored in a blinded manner by one of the authors and by an outside expert in rodent liver pathology (Nanji et al., 1989). The main values of scores were used for statistical analysis.

Histological sections were stained using picrosirius red staining kit (1% Sirius red in saturated picric acid; EasyPath, Indaiatuba, Brazil) for 24 h, or haematoxylin and eosin (Easypath) and examined under light microscopy (Nikon Eclipse 2000 equipped with Nikon DS-Fi2; Nikon Corporation, Tokyo, Japan). For the purpose of quantitative analysis the collagen content, randomly sampled two hundred light microscope images (200X) per liver specimen, including large centrilobular veins and large portal tracts (≥150 mm) were analyzed. About 20 polarized light microscopy images using an Olympus BX60 microscope (Olympus, Tokyo, Japan) (200X) per specimen were captured and analyzed using a color threshold detection system developed in ImageJ (National Institutes of Health). Known positive and negative controls were included in each batch of samples. Tissue reactivity in all groups (negative control, alcohol group and treated group with GNPs) was assessed. Values are expressed as percentage of positive area. Contrast index measurements were obtained from selected area × 100/total area positioned across the regions of interest (three samples per animal). Moreover, hepatic fibrosis was quantified using by (Ishak et al., 1995) scoring system: level 1 indicating the absence of fibrosis; level 2 indicated enlargement of portal area; level 3 was assigned to fibrous expansion of most portal areas; level 4 was assigned to lobules with fibrous expansion of most portal areas with occasional portal to portal bridging; level 5 was assigned to lobules with fibrous expansion of most portal areas with marked bridging (portal to portal and portal to central); level 6 was assigned to lobules with marked bridging (portal to portal and portal to central) with occasional nodules (incomplete cirrhosis); level 7 was observed Cirrhosis in the lobules.

Blood samples collected from the rat and were centrifuged at 3000*g* for 10 min, and resultant supernatants were used to measure the blood alanine aminotransferase level (ALT), aspartate aminotransferase (AST) to evaluate the alcohol-induced liver injury. Liver cytosolic protein solution was used to measure the hepatic triglyceride concentration (mg/g total liver protein, % of control) as a marker of the alcohol-induced lipid surplus in the liver. The levels of ALT and hepatic triglyceride were measured with an automatic analyzer (FDC4000; Fuji Medical Systems, Tokyo, Japan). The data is presented as means with their standard errors (SEM).

3.6. Transmission electronic microscopy

In order to evaluate the uptake of the GNPs by hepatic cells, 0.5 cm fragments were taken from samples of each treatment and fixed in Karnovisky Solution (2.5%) and paraformaldehyde (2.5%) in buffer of 0.1 M cacodylate) for approximately 4 h at 4 °C. After fixation the material was washed with 4× sodium cacodylate (15 min each bath). A drop of 1.6% Potassium Ferrocyanide (FCK) and 2% Osmium Tetroxide for 1 h in a darkroom was added, followed by 2 washes with 0.1 M sodium cacodylate for 15 min and two washes with distilled water. “In block” contrast with 0.5% uranyl acetate in a darkroom for 2 h under refrigeration, dehydrated with acetone in different concentrations, infiltrated and included in resin. Ultra-thin sections (1 μm) are stained with toluidine blue and examined under Zeiss transmission electron microscope, model EM 902 at 80 Kv.

3.7. Immunohistochemical staining

Thin sections of liver (4 μm) were obtained from each group with a microtome and transferred to gelatine-coated slides. Each tissue section was then deparaffinised and rehydrated. The liver tissue slices were washed with 0.3% Triton X-100 in phosphate buffer (PB) and quenched with endogenous peroxidase (3% hydrogen peroxide). Tissue sections were incubated overnight at 4 °C with primary antibodies (Santa Cruz Biotechnology, INTERPRISE, Brazil) against TGF- β, FGF, SOD-1, GPX-1 e IL-1β. Dilution tests (3 dilutions) were performed with all antibodies to identify the 1:800; 1:600; 1:800; 1:1000 and 1:600, dilutions as appropriate, respectively. Slices were washed with phosphate buffer and incubated with a streptavidin/HRP-conjugated secondary antibody (Biocare Medical, Concord, CA, USA) for 30 min. Immunoreactivity to the various proteins was visualized with a colorimetric-based detection kit following the protocol provided by the manufacturer (TrekAvidin-HRP Label + Kit from Biocare Medical, Dako, USA). Sections were counter-stained with hematoxylin. Known positive controls and negative controls were included in each set of samples. Planimetry microscopy (Nikon E200 LED, Morphology Department/UFRN) with a high-power objective (40×) was utilised to score the intensity of cell immunostaining: 1 = absence of positive cells; 2 = small number of positive cells or isolated cells; 3 = moderate number of positive cells; and 4 = large number of positive cells. Labelling intensity was evaluated by two previously trained examiners in a double-blind fashion. Three tissue sections per animal (six animals per group) were evaluated.

3.8. Immunofluorescence microscopy

Three tissue sections from each animal (six animals per group) were deparaffinized in xylene and washed in a series of concentrations of ethanol and PBS. Antigen retrieval was performed by placing the sections in a 10 mM sodium citrate with 0.05% Tween 20 for 40 min at 95 °C. Autofluorescence background noise was reduced by incubating the sections in 0.1% Sudan black in 70% alcohol for 40 min at room temperature (RT). The sections were incubated overnight with rabbit anti-IL-1β, TNF- β and MIF primary antibody (1:200, 1:400 e 1:400 Abcam, EUA and Santa Cruz Biotechnology, USA, respectively), in blocking solution/1% normal goat serum; Abcam, USA and Santa Cruz Biotechnology, USA, respectively) at 4 °C, washed three times in PBS/0.2% triton X-100 for 5 min and incubated with Alexa Fluor 488-conjugated goat anti-rabbit secondary antibody (1:500 in BSA 1%) and DAPI nuclear counterstain (Sigma, USA). Finally, the sections were mounted with Vectashield medium. Fluorescent images were obtained as described by (Araújo et al., 2016).

3.9. Western blot analyses expression

The liver segments were homogenized in RIPA lysis buffer (25 mM Tris-HCL, pH 7.6; 150 mM NaCl; 5 mM EDTA; 1% NP40; 1% triton X-100; 1% sodium deoxycholate; 0.1% SDS) and protease inhibitor (1 μL inhibitor: 100 μL RIPA). For protein extraction, liver samples were centrifuged (17 min, 4 °C, 13000 rpm) and the supernatant was collected. Protein concentrations were determined through the acid assay (Thermo Fisher Scientific) according to the manufacturer‘s protocol. SDS-polyacrylamide gel electrophoresis (10% or 8%) were performed

using 50 μg of protein (previously prepared with sample buffer, BioRad and denatured at 95 °C for 5 min). Then, the protein was transferred to a PVDF membrane (BioRad) for 2 h, blocked with 5% BSA for 1 h, incubated overnight with a primary antibody (mouse anti-β actin, sc-81178, 1:500, Santa Cruz Biotechnology; mouse anti-TGFβ- 1/2-sc80346, 1:200, Santa Cruz Biotechnology; mouse anti-ERK1/ERK2, 136200, 1:500, Invitrogen; Goat anti-Iba-1, ab107159, Abcam) and a secondary antibody (goat anti-rabbit, 656120, Invitrogen, 1:1000; goat anti-mouse IgG, 626520, Invitrogen, 1:500; or rabbit anti-goat, A16142, Invitrogen, 1:1000) for 1 h and 30 min. The membranes were incubated using the ECL system according to the manufacturer's instructions (BioRad) and the chemiluminescence signal was detected using the ChemiDocTM XRS system (BioRad). Densitometric quantification of bands was done through the software ImageJ (NIH, Bethesda, MD, USA).

3.10. Analysis of mRNA expression

Total RNA was extracted from liver tissue with trizol reagent (Invitrogen Co. USA) and the SV Total RNA Isolation System (Promega, Madison, WI). First-strand cDNA was synthesized from 1 μg of total RNA with the ImProm-IITM Reverse Transcriptase System for RT-PCR (Promega) according to the manufacturer's protocol. Real-time quantitative PCR analyses of *GAPDH, PCI, PCIII, NF-Kβ, F4/80, AKT and PI3K* mRNAs were performed with SYBR Green Mix in the Applied Biosystems1 7500 FAST system (Applied Biosystems, Foster City, CA), according to a standard protocol with the following primers of Table 1.

The reference gene for normalization was selected from an analysis of 18S (GenBank sequence NM_003286.2), ubiquitin C (UBC, NM_021009.4), β-actin (ACTB, NM_001101.3) and glyceraldehyde-3-phosphate dehydrogenase (GAPDH, NM_002046.3) genes. GAPDH was chosen as the reference gene because it did not present different amplification patterns (Zhang et al., 2014) As it is a constitutive gene for eukaryotes, the reference gene should not be modified in the disease.

All analyses were performed in a 7500 fast real-time PCR instrument (Applied Biosystems, CA, USA). The standard PCR conditions were as follow: 50 °C for 2 min and 95 °C for 10 min, followed by forty 30-s cycles at 94 °C, a variable annealing primer temperature for 30 s, and 72 °C for 1 min. Reactions were carried in duplicate according to the TaqMan® fast universal PCR master mix (Applied Biosystems, Foster City, CA, USA) protocol in a total volume of 10 μL containing approximately 20 ng cDNA. Mean Ct values were used to calculate the relative expression levels of the target genes for the experimental groups, relative to those in the negative control group; expression data were normalized relative to the housekeeping gene GAPDH using the $2^{-\Delta\Delta Ct}$ formula.

3.11. Statistical analysis

The data is presented as means with their standard errors (SEM) or as medians. Analysis of variance (ANOVA) followed by Bonferroni test was used to in parametric tests. The Kruskal-Wallis and Dunn tests was used to compare medians for non-parametric tests (Graph Pad Prism 5.0 Software, La Jolla, CA, USA).

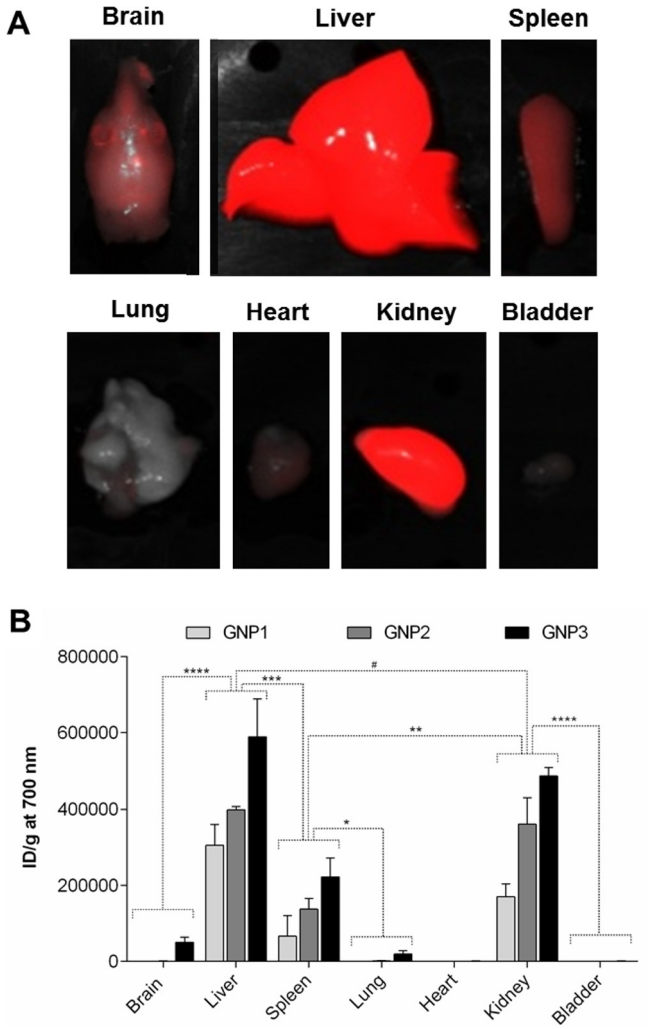

Fig. 1. Tecidual biodistribution of GNPs. Main target organs of GNPs 48 h post i.v. injection of 14 μg/ml (A). Quantitative representation of GNPs distribution intensity at 700 nm in different organs (B). Quantification of GNPs biodistribution in the main organs.

4. Results

4.1. Gnps biodistribution

After I.V. injection of GNPs, we can observe that the liver, kidneys and brain were the tissues where nanoparticles migration occurred most strongly, indicated in Fig. 1A, by greater fluorescence intensity. In the Fig. 1B, shows the quantification of GNPs biodistribution in the main organs and that biodistribution of gold nanoparticles have a dose-dependent effect on the concentrations tested.

Table 1
Primer Sequences used for PCR.

mRNA	Oligonucleotideprimers	Annealing primer temperature
GAPDH	forward: 5′ AAC TTT GGC ATC GTG GAA GG 3′ reverse: 5′ GTG GAT GCA GGG ATG ATG TTC 3′	60 °C
NF-κβ	forward: 5′ TCT GCT TCC AGG TGA CAG TG 3; reverse: 5′ ATC TTG AGC TCG GCA GTG TT 3′	55,2 °C
PCI	forward: 5′ CAG GGA GTA AGG GAC ACG AA 3′;reverse: 5′ TCC CAC AGC AGT TAG GAA CC 3′	56,8 °C
PCIII	forward: 5′ ATG GTG GCT TTC AGT TCA GC 3′;reverse: 5′ TGG GGT TTC AGA GAG TTT GG 3′	55,2 °C
F4/80	forward: 5′ GCC CTT CCA ACT CAT GT 3′ reverse: 5′ AGG GAA TCC TTT TGC ATG TG 3′	55,1 °C
AKT	forward: 5′ TCA CCT CTG AGA CCG ACA CC 3′ reverse: 5′ ACT GGC TGA GGA GAA CTG G 3′	58,5 °C
PI3K	forward: 5′ AAC TTG GCA TGG AAG G 3′,reverse: GTG GAT GCA GGG ATG ATG TTC 3′	55,5 °C

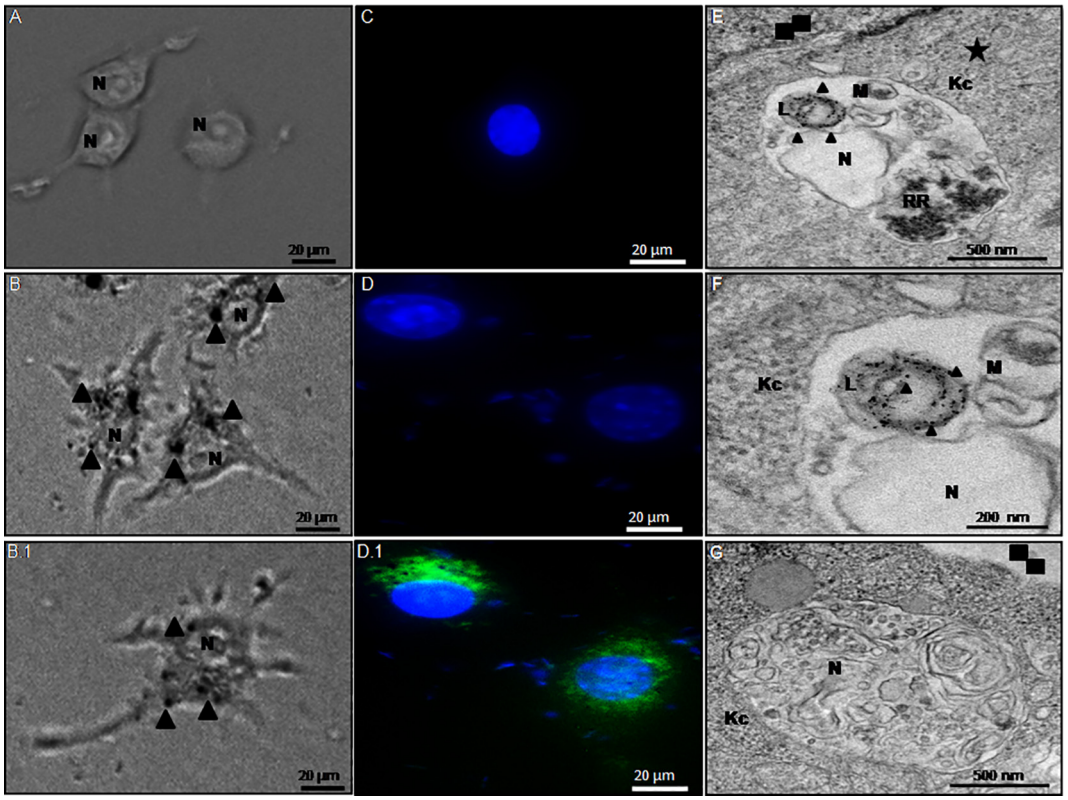

Fig. 2. Intracellular localization of GNPs in macrophage. (B and D.1) and in Kupffer cells Lysossomos (E-G). Negative control, cell without GNPs (A and C). DAPI in blue (C and D) and GNPs in green (D.1). Kc: Kupffer cells; N: nucleus; Triangle: GNPs; L: lysosomes; Star: hepatocyte; Two square: Disse's spaces. Magnification: 400x. Uptake of nanoparticles was evaluated by Fluorescence microscopy (D1). (For interpretation of the references to color in this figure legend, the reader is referred to the web version of this article.)

4.2. Intracellular localization of GNPs in macrophage

In vitro assays were performed in order to investigate how GNPs interact with the cells and whether they are internalized. We observed that GNPs appeared to be internalized by macrophages, likely in the form of agglomerates/aggregates as shown by the light microscopy (Fig. 2B and B.1), and in the spectrum of bright green by immunofluorescence microscopy (Fig. 2D.1). The absence of GNPs in control cells is represented by a lack of agglomerates (Fig. 2A) and absence of the bright green spectrum (Fig. 2C). When the distribution of the GNPs in the liver was evaluated, all mice exposed to GNPs accumulations of nanoparticles were traced in Kupffer cells (Fig. 2E and F), and Fig. 2G. presents a Kupffer cell from the control group that did not receive GNPs. After analyzing the cells and the liver fragments, we observed that the GNPs appear to be primarily localized in the cytoplasm close to nuclei and excluded from them.

4.3. Effects of GNPs on MPO activity and on MDA and GSH levels

Livers from the ethanol + METH group had significantly greater myeloperoxidase (MPO) activity than livers harvested from the saline group ($P < 0.0001$), and this increase was attenuated in the ethanol + METH + GNP3 group that received treatment with 724.96 µg/kg GNPs (Fig. 3A). This same group, in turn, significantly increased glutathione (GSH) levels ($P < 0.0001$) compared to positive control group (Fig. 3C). The malonyldialdehyde (MDA) formation was significantly increased in the ethanol + METH group when compared to saline group ($P < 0.01$) and GNPs treated groups ($P < 0.01$, $P < 0.001$), as seen in Fig. 3B.

4.4. Effect of GNPs treatment on inflammation

The combined treatment with ethanol and METH resulted in increased levels of IL-1β ($P < 0.001$) and TNF-α ($P < 0.001$) compared to saline group (Fig. 3D and E). As noted, such combined treatment may induce side effects which could be reduced by GNPs treatment. Specifically, IL-1β and TNF-α levels in ethanol + METH + GNP3 group were lower than GNPs absence ($P < 0.05$ and $P < 0.001$, respectively). On the other hand, it can also be seen in Fig. 3F, that the combined treatment of ethanol + METH + GNP3 was able to increase IL-10 levels ($P < 0.0001$) compared to ethanol + METH treatment alone.

4.5. Histopathological analysis

At the end of the treatments, the animals were euthanized and their livers excised for histopathological analysis. From then on, after 28 days of saline administration, no pathological changes were observed in the negative control group (Fig. 4A–C), as indexed by a semiquantitative scoring system. However, as seen in Fig. 4E–G, the rats liver from ethanol + METH group exhibited fat accumulation, lymphocytes and neutrophils infiltrate, and necrosis (thin arrows, circle with arrow heads and stars, respectively), resulting in a high pathology scores (Fig. 4M). Additionally, the ethanol + METH group had significantly greater steatosis than the saline group. On the other hand, ethanol and METH-induced liver damage was reduced when associated with GNP3 treatment($P < 0.001$) compared to its respective control without GNPs (Fig. 4G–K). The same effect, however, was not observed for ethanol + METH + GNP1/GNP2 treated groups(Fig. 4I and J). Reduced inflammation was most clearly observed in the ethanol + METH + GNP3 treated group (Fig. 4K), which exhibited decreased areas of steatosis, inflammatory infiltrate contains neutrophils and lymphocytes and reduced levels of necrosis relative to

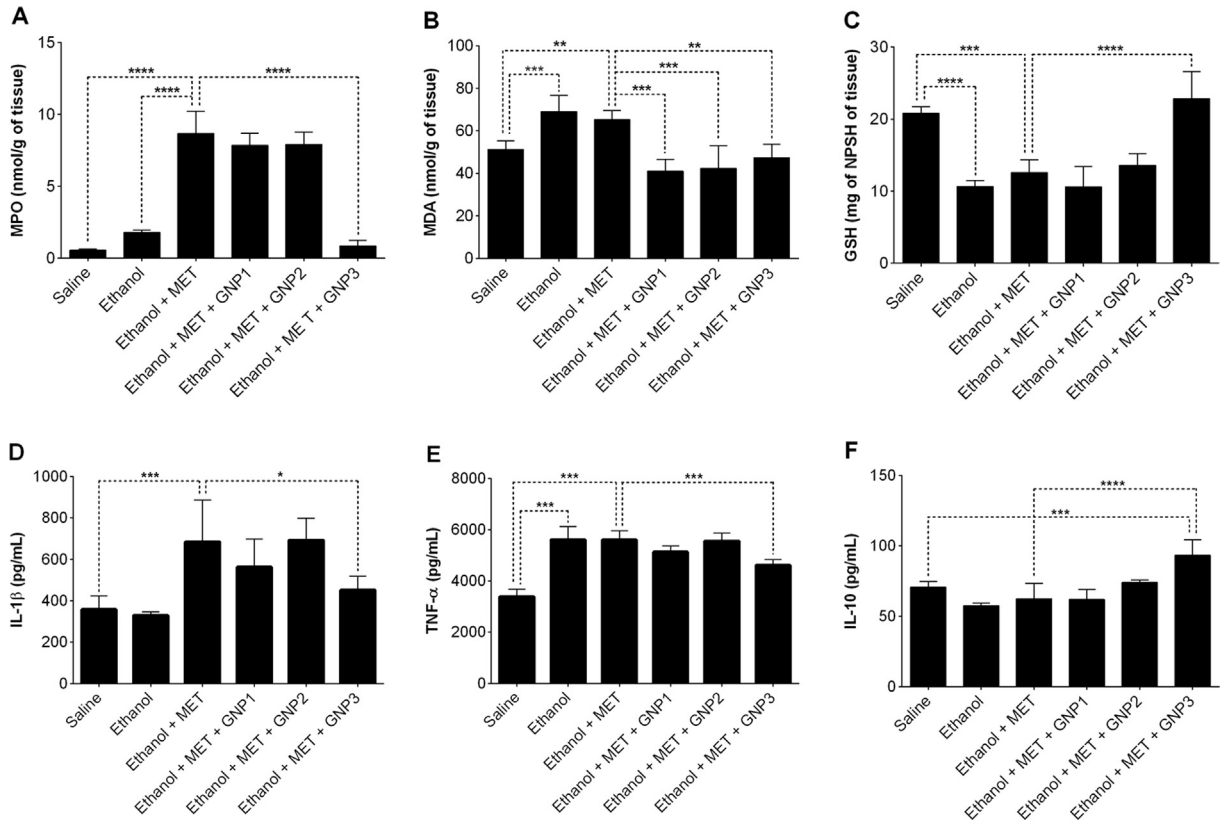

Fig. 3. Modulation of the antioxidant activity and cytokine profile by GNPs. Myeloperoxidase activity (MPO) (A), malondialdehy deformation (MDA) (B), and reduced glutathione levels(GSH) (C). Cytokine analysis(D–F). METH, methamphetamine; GNP1, gold nanoparticles 181.48 μg/kg; GNP2, gold nanoparticles 362.48 μg/kg, GNP3, gold nanoparticles 724.96 μg/kg. $^{*}p < 0.05$; $^{**}p < 0.01$; $^{***}p < 0.001$; $^{****}p < 0.0001$.

ethanol + METH group alone.

Negative control group livers had weak staining limited to centrilobular veins as shown in the Fig. 4D. Liver sections from the positive control group exhibited marked portal fibrosis and staining between the hepatic cords (Fig. 4H). The treated group with GNP3 had a significative ($P < 0.01$) fibrotic response as can be seen when comparing Fig. 4H, L and M. Morphometric quantification of Sirius red stained areas demonstrated an attenuation of the fibrotic process in the treated group compared to the positive control group. Fig. 4M shows that treatment of the GNP3 group had an attenuation of the fibrotic process in the liver, according to the analysis of the tissue fractions with the application of the Ishak scores.

In addition, treatment with ethanol and METH combined with GNP3 was able to reduce the AST, ALT and hepatic triglycerides levels (Fig. 5A–C) when compared to the control groups. However, GNPs treatment modulated this ethanol and METH-induced hepatosteatosis and liver injury (Fig. 5). After analyzing the data of ALT, AST, hepatic Triglycerides, pro-and anti-inflammatory cytokines, anatomopathological analysis, we concluded that among the 3 doses tested the GNP3 was the one that presented the best results, therefore the following tests as Immunohistochemistry, Immunofluorescence, Electronic Microscopy RT-PCR-*Real Time*, Western Blot, were performed only with the negative and postoperative control groups and the group treated with the best dose of GNPs (GNP3).

4.6. Immunohistochemistry and immunofluorescence

The histopathological analysis was followed with antibody labeling for transforming growth factor-beta (TGF-β), fibroblast growth factor (FGF), SOD-1 and GPX-1 observation. When compared to alone ethanol + METH exposure, the ethanol + METH + GNP3 group was able to reduce the TGF-β, FGF, SOD-1 ($P < 0.001$) and GPX-1 levels ($P < 0.01$), as observed in the Fig. 6 and 7. These changes were consistent with the normalization toward non-ethanol and METH exposure levels.

Evaluation of IL-1β, TNF-α and macrophage migration inhibitory factor (MIF) was carried out by labelling with antibodies conjugated with fluorescent agent. Cellular IL-1β, TNF-α and MIF labelling (green) were strong and diffuse in the ethanol + METH group(Fig. 8B, E and H), poorly marked in the ethanol + METH + GNP3 group (Fig. 8C, F and I), and absent in saline group (Fig. 8A, D, and G). Densitometric analysis confirmed that there were significantly increased IL-1β, TNF-α and MIF immunoreactivities in the ethanol + METH group, relative to the saline group, and lower immunoreactivity in the ethanol + METH + GNP3 group(Fig. 8J, K, and L).

4.7. Gnps treatment decreased NF-κB, F480, AKT, PI3K, PCI and PCIII mRNA expression

For all evaluated genes the relative mRNA expression was decreased when the groups were treated with ethanol + METH + GNP3 in relation to their respective control without the GNP3 ($P < 0.0001$ or $P < 0.001$), as observed in Fig. 9A–F.

4.8. IBA-1, ERK1/ERK2 and TGF-β expression

The final product of ionized calcium-binding adaptor molecule 1 (IBA-1), ERK1/ERK2 and TGF-β genes expression into rats liver, exposed to ethanol + METH, was evaluated by western blot as show Fig. 9G. Increased expression of IBA-1, ERK1 and TGF-β and decreased expression of ERK2in the ethanol + METH + GNP3 group were observed. The final product of IBA, ERK1/ERK2 and TGF-β genes expression into rats' liver, exposed to ethanol + METH, was evaluated by western blot as show Fig. 9G. Increased expression of IBA-1, ERK1 and

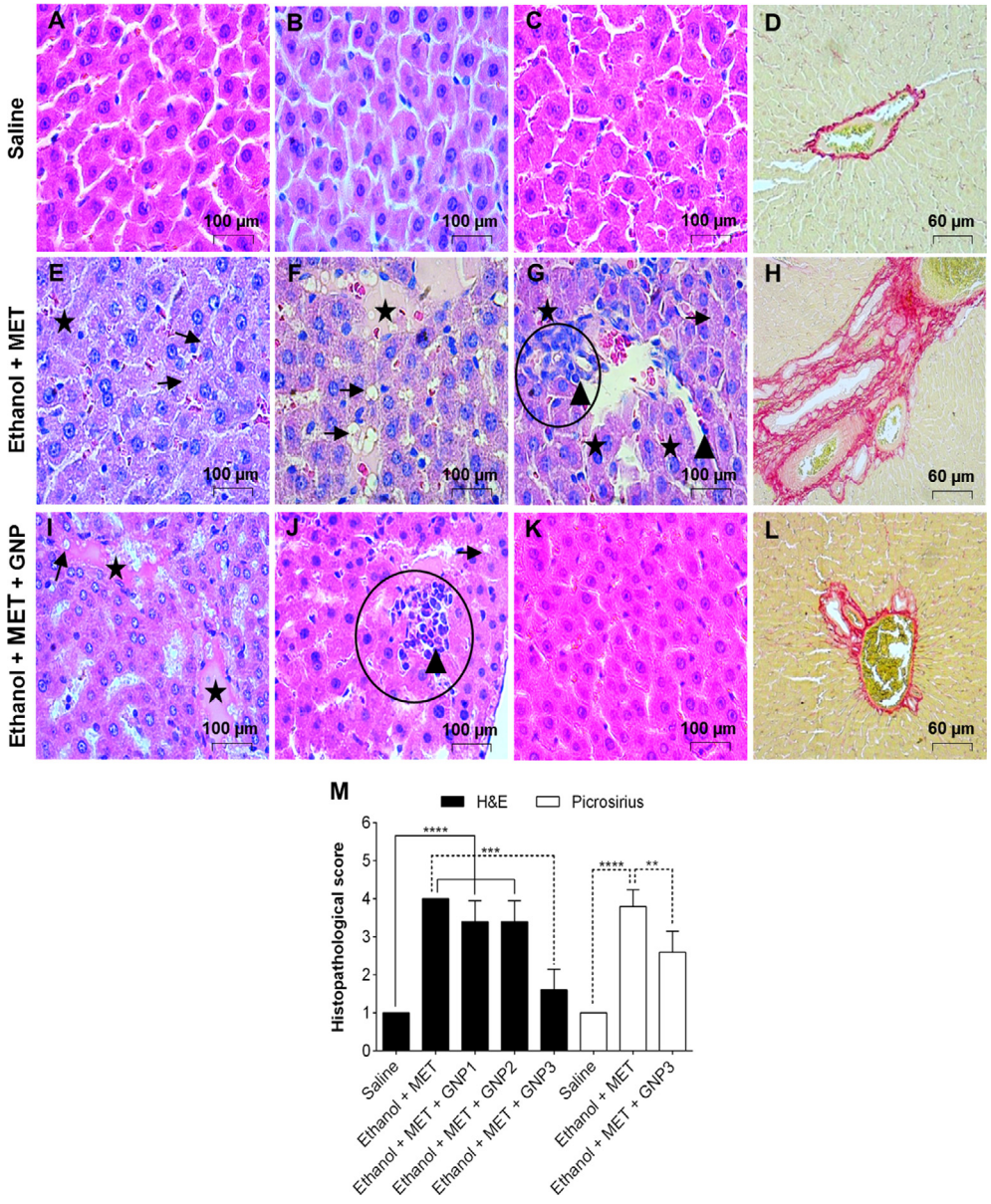

Fig. 4. Histological analysis from hepatic parenchyma. Group treated with saline solution (A–D), alcohol 30% + methamphetamine (METH) (E–H) and groups treated with GNP1 191.24 µg/kg (I), GNP2 362.8 µg/kg (J), GNP3 724.96 µg/kg (K-L). Fibrosis analysis by Picrosirius staining (D, H and L). The area fraction of total fibrosis, including fibrosis in the portal tract area, in rats with GNP3 group induced liver injury in relation to the Ishak score. Graphical representation of the mean histopathological score from each treated group (M). Arrow, fatty changes within hepatocytes; arrow head, neutrophils; star: necrosis area; circle, lymphocytes and neutrophils infiltrate. Magnification 400×. $^{*}p < 0.05$; $^{**}p < 0.01$; $^{***}p < 0.001$; $^{****}p < 0.0001$.

TGF-β and decreased expression of ERK2 in the ethanol + METH + GNP3 group were observed. No overexpression of IBA-1, ERK1 and TGF-β, already in the positive control group we observed intense marking intense labeling of the analyzed proteins.

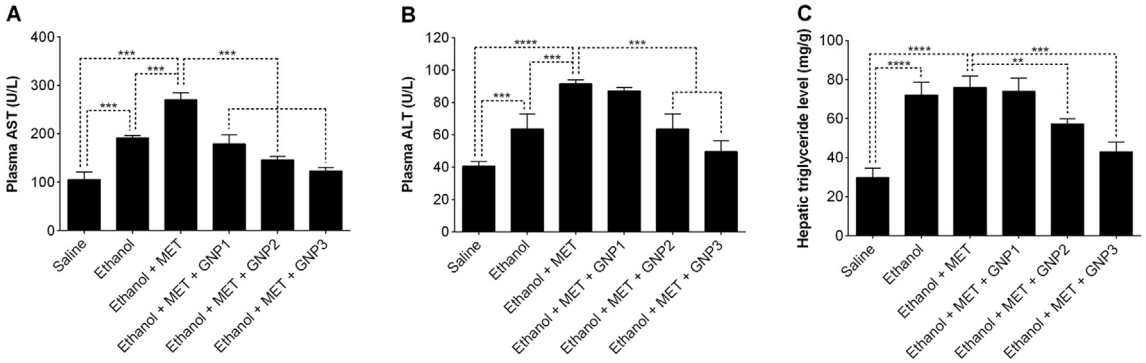

Fig. 5. Biochemical assessments of liver function. (A) Aspartate aminotransferase (AST), (B) Alanine aminotransferase(ALT). (C) Triglyceride. METH, methamphetamine; GNP1, gold nanoparticles 181.48 µg/kg; GNP2, gold nanoparticles 362.48 µg/kg, GNP3, gold nanoparticles 724.96 µg/kg. $^{**}p < 0.01$; $^{***}p < 0.001$; $^{****}p < 0.0001$).

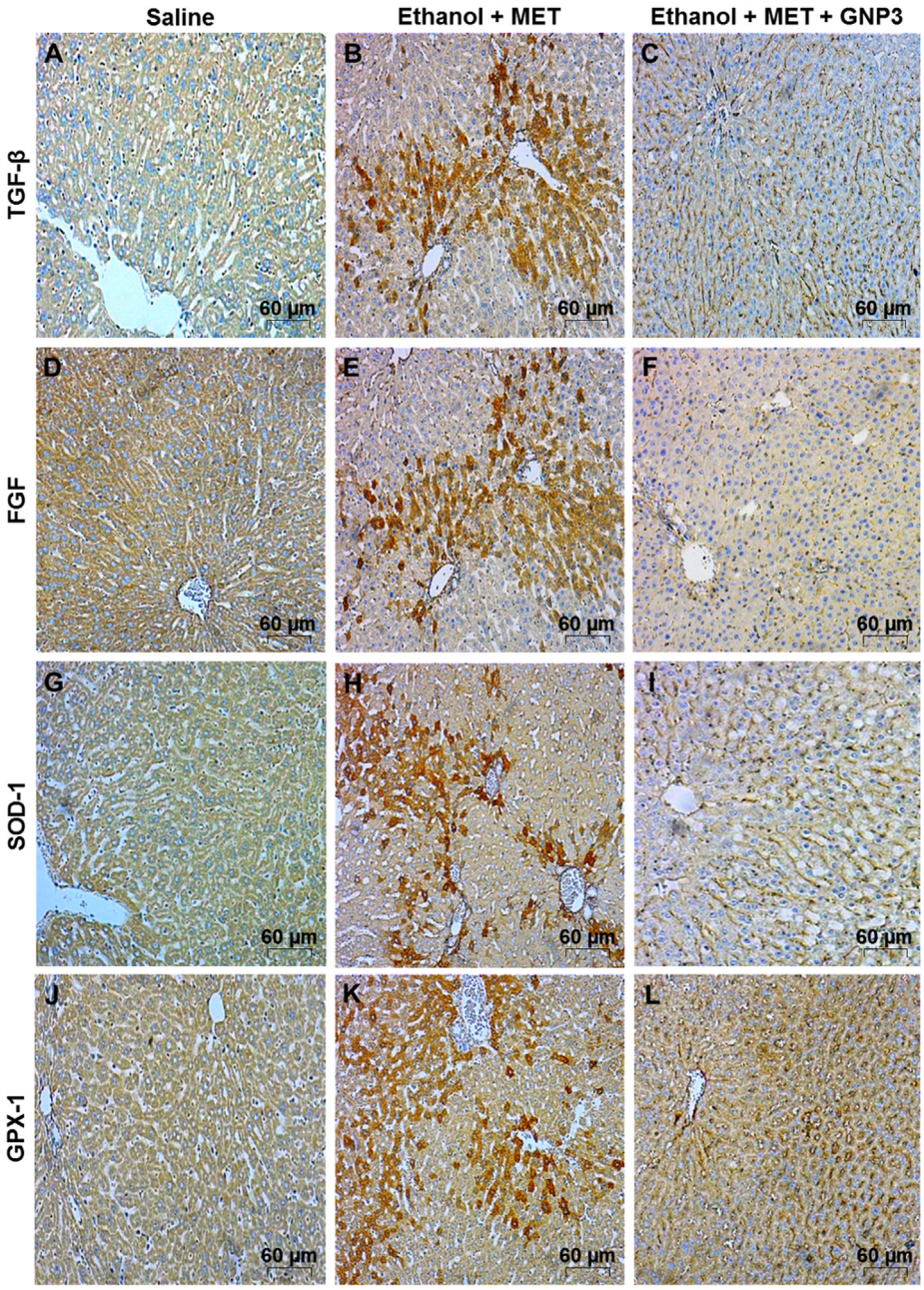

Fig. 6. Immunohistochemicalanalysis from hepatic parenchyma. The saline (A, D, G, and J), alcohol + methamphetamine (B, E, H and K) and alcohol + methamphetamine + GNP 724.96 µg/kg (C, F, I and L) groups were labeled for evaluation of TGF-β(A-C) and FGF (D-F) growth factors, and for oxidative stress through SOD-1(G-I) and GPX-1 (J-L). METH, methamphetamine; GNP3, gold nanoparticles 724.96 µg/kg. Magnification 400×.

5. Discussion

This study is the first into examine the anti-inflammatory, antioxidant and anti-fibrotic activity of GNPs in a rat model after ethanol and METH-induced liver injury through an analysis of markers of the inflammatory, oxidant and fibrotic processes. This was perfectly evidenced by a significant increase in several biochemical parameters such as oxidative stress, biomarkers of inflammation, severe fat accumulation, necrosis and accumulation of collagen type I and III around the hepatic triad which resulting in an strong steatosis beyond elevated neutrophil, MPO, and pro-inflammatory cytokine levels were also found all these changes were well evidence in the positive control groups.

When comparing the results obtained in this research with the results obtained previously (de Araújo et al., 2017), we have noticed that the dose used and the size of the GNPs are a key factor for effectiveness in the treatment with GNPs. Previously our group, observed that the highest GNPs dose (1500 µg/kg) generated 49% of reduction in leukocyte migration, which attested the activation of a cellular anti-inflammatory response, while the groups received GNPs showed decreases levels in the pro-inflammatory cytokine IL-1β(700 and 1500 µg/kg, $P < 0.05$) and TNF-α(700, 1000 and 1500 µg/kg, $P < 0.001$) compared to positive control group (Araújo et al., 2017). Other studies also showed this relation of importance of the size of GNP and increased expression of proinflamatory cytokines (Khan et al., 2013; Ibrahim et al., 2018).

From the biodistribution tests, we have shown that after 48 h GNPs migrated mainly to the spleen, kidney and liver, reaching 2×10^5, 5×10^5 and 6×10^5 ID/g, respectively, corroborating with the results seen earlier (de Araújo et al., 2017) and evidencing that after administration these GNPs migrate to the nucleus of Kupffer cells in the liver.

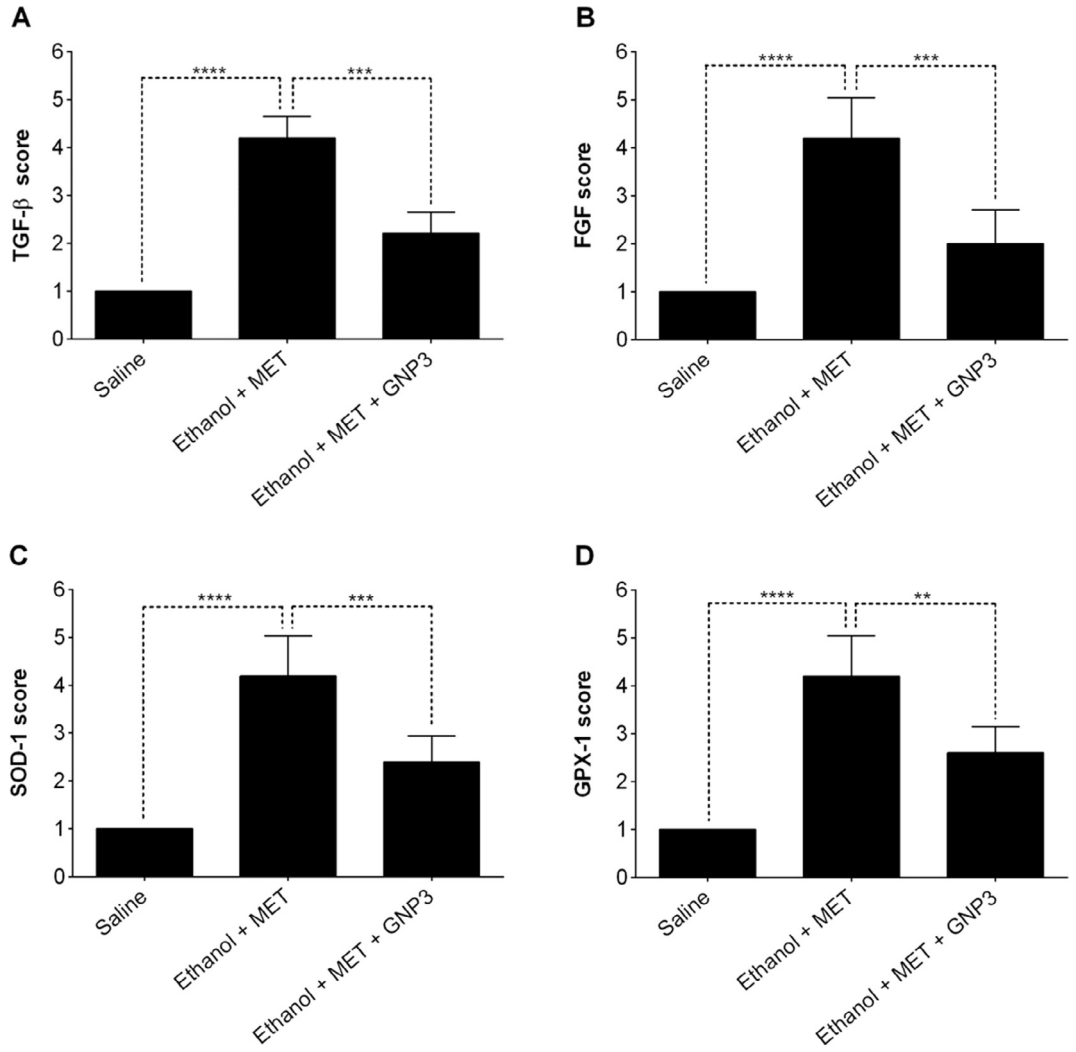

Fig. 7. Immunohistochemistry scores. Graphical representation of the mean scores from alcohol + methamphetamine + GNP 724.96 μg/kg treated group for TGF-β (A), FGF (B), SOD-1 (C) and GPX-1 (D) immunoreactivity. $^{**}p < 0.01$; $^{***}p < 0.001$; $^{****}p < 0.0001$.

Studies have shown that the extent of cerebral uptake of anionic nanoparticles is higher than cationic and neutral GNPs (Noor et al., 2016; Goodman et al., 2004). In this way, the surface of the NPs should be considered in the neurotoxicity profile and in the distribution, since neutral charges present irrelevant neurotoxicity (Masserini, 2013). Not all types of nanoparticles are feasible for use in a strategy whose objective is to cross the blood-brain barrier (BBB). Surface characteristics vary depending on the nanomaterials used and it was found that neutral nanoparticles and low concentrationanionic effects have no effect on this barrier (De Jong and Borm 2008).

In previous studies, we observed that results indicated that GNPs at the low concentrations below to 2 ppm did not show any toxicity, but at the higher concentrations, significant changes were observed in the organ (Araújo et al., 2017; Zhang et al., 2010; Mironava et al., 2010). However, this accumulation of GNPs in the liver did not cause any morphological changes in this organ (de Araújo et al., 2017). GNPs (13 nm in diameter) after 28 days existed with the amount of 1.5%–9.2% in the kidneys, while the amount is negligible in the urine (Yang et al., 2007). Extreme changes in the histopathology of lung and liver tissues caused by spherical GNPs with 5–10 nm size in 5 (5000 μg/kg), 10 (10.000 μg/kg), and 100 (100.0000 μg/kg) ppm treatment groups, been the pathological changes (lung and liver tissue) in treatment group (Au 100 ppm) more intense compared to the other groups (Abdelhalim et al., 2011). However, in this work was used 0,724 ppm GNPs in the treatment groups. However, in our work was used dose of 0,724 (724 μg/kg) ppm GNPs in the treatment groups in the groups that presented the best results.

Some works have showed a non-immunogenic character of the GNPs or have even proven their anti-inflammatory effect, consisting of the reactive oxygen and nitrite species inhibition as well as pro-inflammatory cytokines in macrophages (Kurniawan et al., 2017; Zhang et al., 2011). *In vivo* experiments also conducted on several animal models of inflammatory conditions have confirmed the anti-inflammatory and antioxidant properties of the GNPs, manifested by a decrease in the levels of pro-inflammatory cytokines (IL-1β,TNF-α) and oxidative tissue damage markers (Araújo et al., 2017; Tsai et al., 2012; Dohnert et al., 2012; Sumbayev et al., 2013).

Oxidative stress is known to play a crucial role in METH-induced toxicity in the brain and other tissues, as evidenced by previous studies. However, a comparison of oxidative effects of MET in different organs has not been sufficiently studied previously (Tokunaga et al., 2006). It has been suggested that the hepatic catalase level is negatively associated with the severity of alcoholic liver injury (de Araújo et al., 2016; Powell et al., 2010) and that SODs scavenge hydroxyl peroxides generated in the cytosol and mitochondria, thereby terminating autoxidation. Gold nanoparticles can increase the anti-oxidant defense enzymes and creating a sustained such as GSH, SOD, Catalase and GPx in diabetic mice to normal, by inhibition of lipid peroxidation and ROS generation (Barathmanikanth et al., 2010). In this work, ethanol associated to METH imbalanced the hepatocellular antioxidant system,

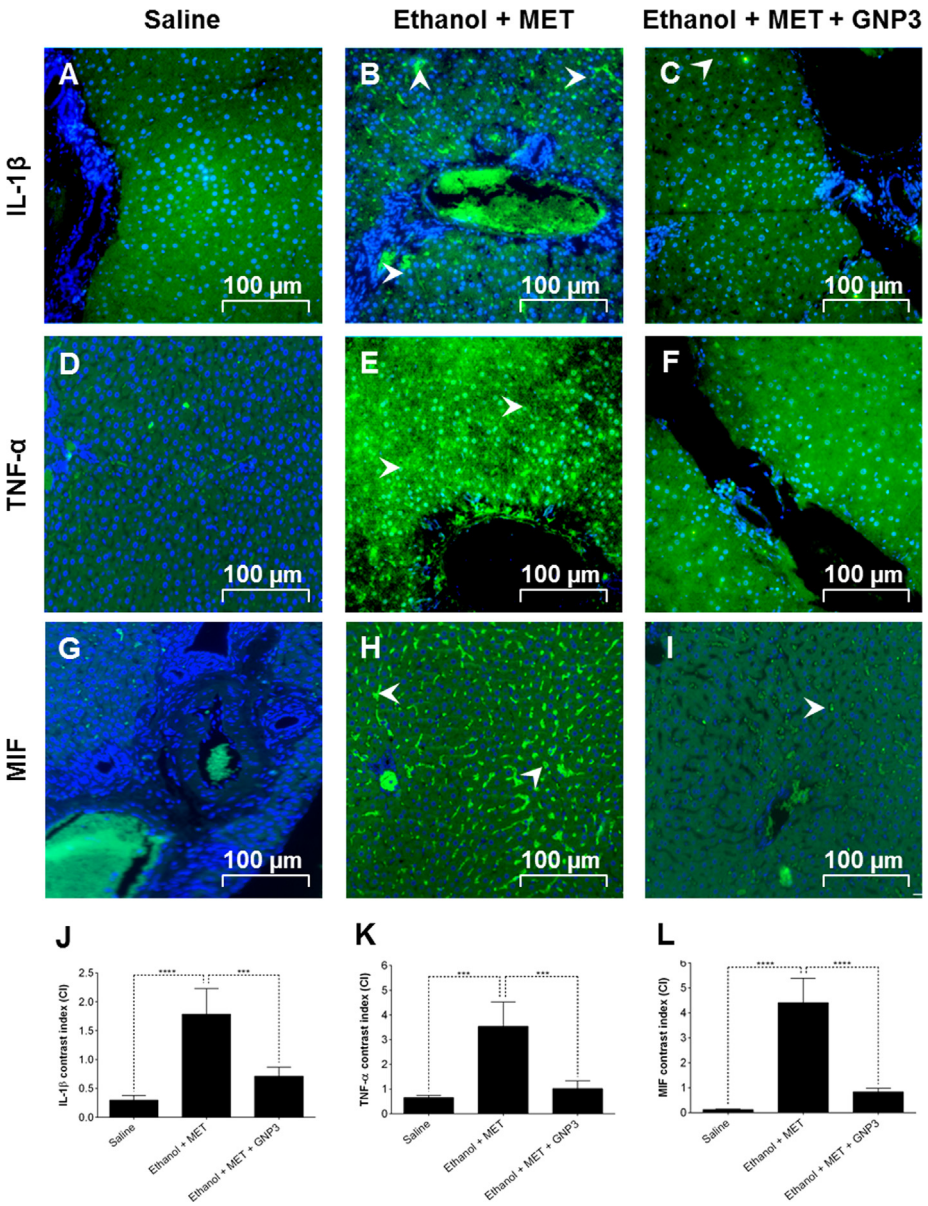

Fig. 8. Modulation of expression of IL-1β, TNF-α and MIF. Representative photomicrographs of IL-1β(A-C), TNF-α(D-F) and MIF(G-I) immunoreactivity in liver specimens from each group (green) with DAPI nuclear counterstained (blue). Graphical representation of the contrast index from IL to 1β (J), TNF-α (K) and MIF (L). METH, methamphetamine; GNP3, gold nanoparticles 724.96 µg/kg. $^{***}p < 0.001$; $^{****}p < 0.0001$. (For interpretation of the references to color in this figure legend, the reader is referred to the web version of this article.)

inflammatory cytokines and liberated the free radicals (Khan et al., 2012), as evidenced by the decrease in GSH level and the increased levels of MDA and MPO in hepatic tissue. GNPs724.96 µg/kg, however, increased hepatic GSH level and SOD-1 and GPX-1 expression, as well as decreased the MDA and MPO levels. Other studies in model of acute peritonitis study suggest that gold NPs of 10 nm diameter produce significant lipid peroxidation in rat liver however lungs and heart do not show any oxidative stress (Khan et al., 2012). That probably do not apply to our GNPs because they are smaller in size.

Ethanol pre-treatment was also able to exacerbate METH-induced hepatotoxicity, which could be ascertained by the significant increase of plasma transaminases activities, (hepatic lesion biomarkers), when animals were exposed to ethanol and METH. The increase in AST, ALT and triglycerides levels were already described for both compounds in humans (Ellis et al., 1996; Yue et al., 2006) and rats (Beitia et al., 2000; Montet et al., 2002). Increased prostaglandin E_2 (PGE_2) causes triglycerides accumulation in hepatocytes, and therefore, a state of steatosis (Bautista, 2002). This hepatotoxic effect was also confirmed by the decrease in liver weight when METH was administered to ethanol pre-exposed rats and by histological analysis of liver sections by light and electron microscopy, which gives further evidences that the concomitant exposure to METH and ethanol results in a marked aggravation of the hepatotoxic effects such as fat accumulation, lymphocytes and neutrophils infiltrate, necrosis and fibrosis (Araújo et al., 2016). GNPs724.96 µg/kg, in turn, reduced all these histopathologic features.

Hepatocyte apoptosis causes recruitment of inflammatory cells to damaged liver and release of pro-fibrogenic cytokines (TGF-β1, IL-6, IL-1β, TNF-α) (Potter and Mezey, 2007; Seki et al., 2007). IL-10 is a potent anti-inflammatory molecule that has been shown to inhibit TNF-α and IL-1 cytokines production and to suppress NF-κB activation (Mandal et al., 2010). IL-10 reduces nitric oxide and reactive oxygen intermediates macrophage production, and also reduces adhesion molecules and chemokines expression (Gao, 2012). Bone marrow(BM)-derived and liver resident macrophages (Kupffer cells, KC) produce TGF-β1 in

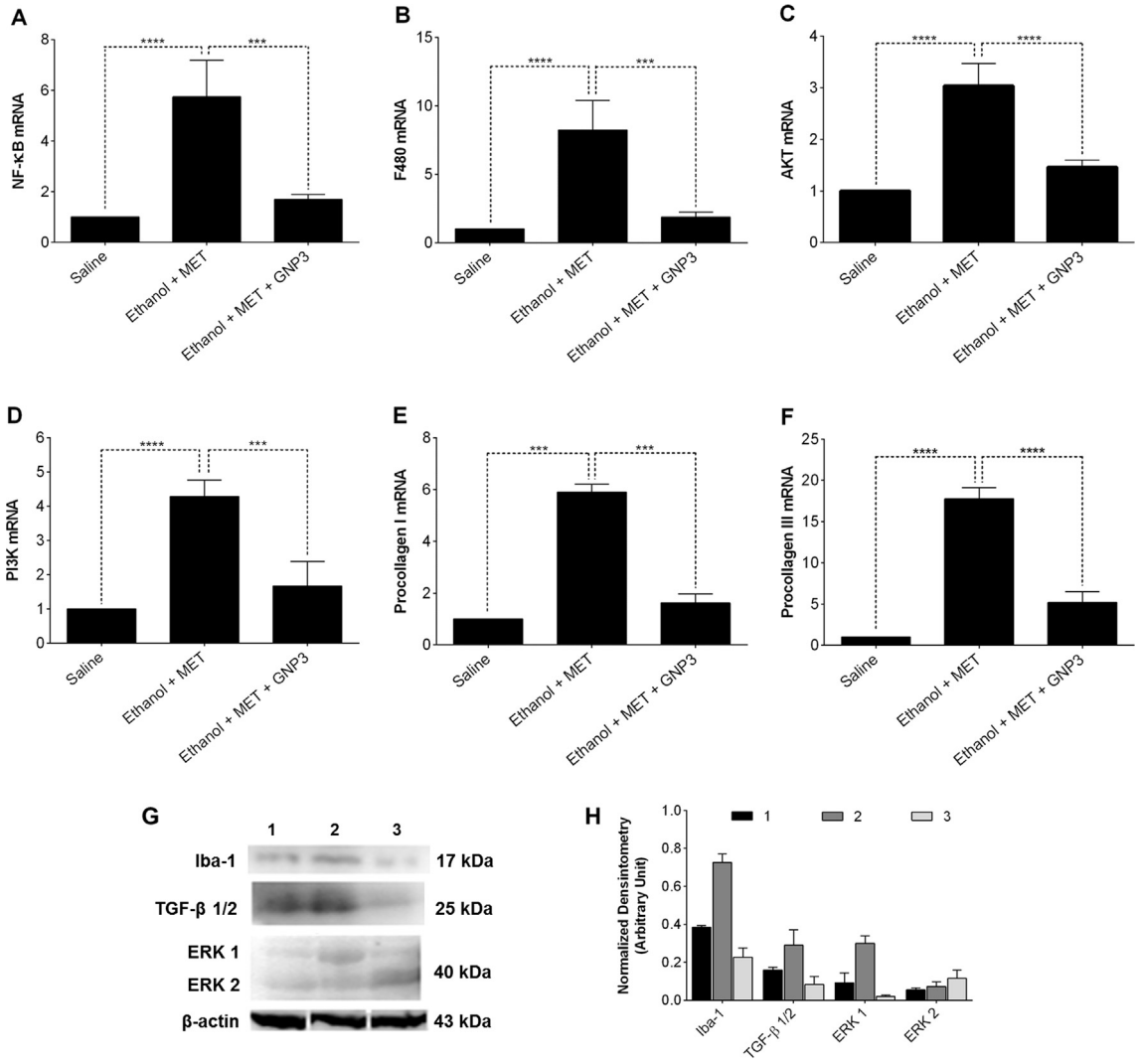

Fig. 9. Gene expression at mRNA and protein levels. Relative mRNA expression fromNF-κB (A), F480 (B), AKT (C), PI3K (D), Procollagen I (E) and Procollagen III (F) genes. Results are presented as fold-change of the media values, normalized to glyceraldehyde 3-phosphate dehydrogenase (GAPDH) and expressed by mean ± SEM ($^{**}p < 0.001$; $^{****}p < 0.0001$). Protein expression from IBA-1, ERK1/ERK2 and TGF-β genes (Fig. 9G) was detected in total protein extracts determined by western blot, with detection of β-actin used as a loading control. Graphical representation densitometry analysis the result of analysis western blot (Fig. 9H). METH, methamphetamine; GNP3, gold nanoparticles 724.96 μg/kg. In Fig. 9G Figs. 1–3 represent the analyzed groups 1-negative control group, 2-positive control group and 3 group treated with GNPs 724.96 μg/kg. Data were representative of at least two similar experiments.

the fibrotic liver (Potter and Mezey, 2007). TGF-β1 is a critical for activation of fibrogenic myofibroblasts, which in response to injury up-regulate α-smooth muscle actin (α-SMA) and secrete extracellular matrix proteins, mostly collagen Type I (Col) (Seki et al., 2007).

Hepatic stellate cells (HSCs) are the major source of fibrogenic myofibroblast in liver injury. There is an overwhelming evidence that activated HSCs are the major producers of the fibrotic matrix and that HSC apoptosis is the primary mechanism of regression of liver fibrosis (Kweon et al., 2003). Inflammation is the main characteristic in liver fibrosis and KCs are considered to be the primary source of inflammatory cytokines (Nieto, 2006). In this study, we show that IL-1β, TNF-α levels and PCI and PCIII mRNA expression were increased while IL-10 cytokine was decreased in ethanol + METH group alone. On the other hand, inverted results were found in the 724.96 μg/kg GNPs. Besides, our findings show that GNPs724.96 μg/kg treatment inhibited NF-κB mRNA expression significantly.

The stimulatory effect of macrophage migration inhibitory factor (MIF) is, at least partly, dependent on IL-1β and IL-23 production, and involves the signaling pathways of MAP kinase (MAPK) (Gordon et al., 2014). The activated PI3-K participate in regulation of HSC migration, proliferation, collagen secretion and adhesion(Friedman, 2000) besides being involved in regulating a number of cellular responses, such as cell growth, survival and migration. The AKT is downstream of PI3-K and activation of AKT is associated with HSC proliferation and α1 (I) collagen transcription and translation (Reif et al., 2003). In the liver, macrophage-associated PI3K activation promotes cytokine production and subsequent hepatocyte proliferation early following partial hepatectomy (Jackson et al., 2008). Hepatocyte-associated PI3K regulates growth following a reduction in the liver volume, a process involving AKT activation. The activated PI3K/AKT was found to participate in regulation of HSC migration, proliferation, collagen secretion, and adhesion (Reif et al., 2003; Aslan et al., 2004). In the present work, GNPs 724.96 μg/kg inhibited macrophage-specific adhesion (F4/80), PI3K and AKT mRNA expression.

Compared with GNPs, negatively charged were retained longer in liver and spleen, presumably due to internalization by Kupffer cells and macrophages causing the formation of oxygen reaction species (Wang et al., 2016). GNPs appear to a type of be one of the promising treatment for hepatic injury, when the GNPs enter in the bloodstream, they are trapped by the Kupffer cells in the liver, or if smaller than about

4–6 nm partially be filtrated into the preurine (Sadauskas et al., 2007; Sereemaspun et al., 2008) where the nanoparticle retention in the liver and spleen is low suggesting elimination through the kidneys. This mechanism seems to be very efficient and capable of protecting the rest of the organism from the nanoparticles (Sadauskas et al., 2007).

In our study, we showed that 724.96 μg/kg GNPs down-regulated the activity of Kupffer cells and hepatic stellate cells affecting the profile of their pro-inflammatory cytokines, oxidative stress and fibrosis through modulation of signaling pathways AKT/PI3K and MAPK.

Acknowledgments:

The authors are grateful to the Brain Institute (Federal University of Rio Grande do Norte) and the Leiden University Medical Center for their contributions to the present study. We acknowledge support by postdoctoral fellowship from the Raimundo Fernandes de Araujo Junior by CAPES 88881.119850/2016-01 and the European Commission where RFde A, ABC and LJC have received funding from a MSCA-ITN-2015-ETN Action grant (proposal number: 675743; project: ISPIC).

Conflict of interest statement

The authors declare no conflicts of interest.

References

Abdelhalim, K. Mohamed Anwar, Jarrar, Bashir M., 2011. Gold nanoparticles induced cloudy swelling to hydropic degeneration, cytoplasmic hyaline vacuolation, polymorphism, binucleation, karyopyknosis, karyolysis, karyorrhexis and necrosis in the liver. Lipids Health Dis. 10 (1), 166. http://dx.doi.org/10.1186/1476-511X-10-166.

Almalki, Atiah H., Das, Sujan C., Alshehri, Fahad S., Althobaiti, Yusuf S., Sari, Youssef, 2018. Effects of sequential ethanol exposure and repeated high-dose methamphetamine on striatal and hippocampal dopamine, serotonin and glutamate tissue content in wistar rats. Neurosci. Lett. 665 (Supplement C), 61–66. http://dx.doi.org/10.1016/j.neulet.2017.11.043.

Araújo, Raimundo Fernandes, De, Vinícius Barreto, Garcia, Renata Ferreira, Leitão, De Carvalho, Brito, Gerly Anne De Castro, De Castro, Emilio, Miguel, Paulo Marcos, Guedes, Matta, Araújo, Aurigena Antunes De, 2016. Carvedilol improves inflammatory response, oxidative stress and fibrosis in the alcohol-induced liver injury in rats by regulating kuppfer cells and hepatic stellate cells. PLoS One 11 (2). http://dx.doi.org/10.1371/journal.pone.0148868.

Araújo, Raimundo Fernandes, de, de Araújo, Aurigena Antunes, Pessoa, Jonas Bispo, Freire Neto, Franscisco Paulo, da Silva, Gisele Ribeiro, C.S. Leitão Oliveira, Ana Luiza, de Carvalho, Thaís Gomes, et al., 2017. Anti-inflammatory, analgesic and anti-tumor properties of gold nanoparticles. Pharmacol. Rep. 69 (1), 119–129. http://dx.doi.org/10.1016/j.pharep.2016.09.017.

Aslan, Kadir, Lakowicz, Joseph R., Geddes, Chris D., 2004. Nanogold-plasmon-resonance-based glucose sensing. Anal. Biochem. 330 (1), 145–155. http://dx.doi.org/10.1016/j.ab.2004.03.032.

Barathmanikanth, Selvaraj, Kalishwaralal, Kalimuthu, Sriram, Muthuirulappan, Pandian, Sureshbabu Ram Kumar, Youn, Hyung-Seop, Eom, Soohyun, Gurunathan, Sangiliyandi, 2010. Anti-oxidant effect of gold nanoparticles restrains hyperglycemic conditions in diabetic mice. J. Nanobiotechnol. 8, 16. http://dx.doi.org/10.1186/1477-3155-8-16.

Bartneck, M., Warzecha, K.T., Tacke, F., 2014. Therapeutic targeting of liver inflammation and fibrosis by nanomedicine. Hepatobiliary Surg. Nutr. 3 (6), 364–376. http://dx.doi.org/10.3978/j.issn.2304-3881.2014.11.02.

Bautista, A.P., 2002. Acute ethanol binge followed by withdrawal regulates production of reactive oxygen species and cytokine-induced neutrophil chemoattractant and liver injury during reperfusion after hepatic ischemia. Antioxid. Redox Signalling 4 (5), 721–731. http://dx.doi.org/10.1089/152308602760598864.

Beitia, G., Cobreros, A., Sainz, L., Cenarruzabeitia, E., 2000. Ecstasy-induced toxicity in rat liver. Liver 20 (1), 8–15. http://dx.doi.org/10.1034/j.1600-0676.2000.020001008.x.

Chen, Ya-Ling, Chen, Li-Ju, Bair, Ming-Jong, Yao, Mei-Lan, Peng, Hsiang-Chi, Yang, Sien-Sing, Yang, Suh-Ching, 2011. Antioxidative status of patients with alcoholic liver disease in Southeastern Taiwan. World J. Gastroenterol.: WJG 17 (8), 1063–1070. http://dx.doi.org/10.3748/wjg.v17.i8.1063.

De, Mrinmoy, Rotello, Vincent M., 2008. Synthetic 'chaperones': nanoparticle-mediated refolding of thermally denatured proteins. Chem. Commun. (Cambridge, England) 30, 3504–3506. http://dx.doi.org/10.1039/b805242e.

Dohnert, Marcelo B., Venâncio, Mirelli, Possato, Jonathann C., Zeferino, Rodrigo C., Dohnert, Luciana H., Zugno, Alexandra I., De Souza, Cláudio T., Paula, Marcos M S, Luciano, Thais F., 2012. Gold nanoparticles and diclofenac diethylammonium administered by iontophoresis reduce inflammatory cytokines expression in achilles tendinitis. Int. J. Nanomed. 7, 1651–1657. http://dx.doi.org/10.2147/IJN.S25164.

Dykman, L.A., Bogatyrev, V.A., 2000. Use of the dot-immunogold assay for the rapid diagnosis of acute enteric infections. FEMS Immunol. Med. Microbiol. 27 (2), 135–137.

Ellis, A.J., Wendon, J.A., Portmann, B., Williams, R., 1996. Acute liver damage and ecstasy ingestion. Gut 38 (3), 454–458. http://dx.doi.org/10.1136/gut.38.3.454.

Esterbauer, Hermann, Cheeseman, Kevin H., 1990. Determination of aldehydic lipid peroxidation products: malonaldehyde and 4-hydroxynonenal. Methods Enzymol. 186 (C), 407–421. http://dx.doi.org/10.1016/0076-6879(90)86134-H.

Friedman, S.L., 2000. Molecular regulation of hepatic fibrosis, an integrated cellular response to tissue injury. J. Biol. Chem. 275 (10), 2247–2250. http://dx.doi.org/10.1074/jbc.275.4.2247.

Fröhlich, Eleonore, 2012. The role of surface charge in cellular uptake and cytotoxicity of medical nanoparticles. Int. J. Nanomed. http://dx.doi.org/10.2147/IJN.S36111.

Gao, Bin, 2012. Hepatoprotective and anti-inflammatory cytokines in alcoholic liver disease. J. Gastroenterol. Hepatol. 27 (Suppl 2), 89–93. http://dx.doi.org/10.1111/j.1440-1746.2011.07003.x.

Gasparotto, Luiz H S, Garcia, Amanda C., Gomes, Janaina F., Tremiliosi-Filho, Germano, 2012. Electrocatalytic performance of environmentally friendly synthesized gold nanoparticles towards the borohydride electro-oxidation reaction. J. Power Sources 218, 73–78. http://dx.doi.org/10.1016/j.jpowsour.2012.06.064.

Goodman, Catherine M., McCusker, Catherine D., Yilmaz, Tuna, Rotello, Vincent M., 2004. Toxicity of gold nanoparticles functionalized with cationic and anionic side chains. Bioconjug. Chem. 15 (4), 897–900. http://dx.doi.org/10.1021/bc049951i.

Gordon, Siamon, Plüddemann, Annette, Estrada, Fernando Martinez, 2014. Macrophage heterogeneity in tissues: phenotypic diversity and functions. Immunol. Rev. 262 (1), 36–55. http://dx.doi.org/10.1111/imr.12223.

Gunes, Y., Y, L.Y., Gumrukcuoglu, H.A., Tuncer, M., 2010. Role of echocardiography in the evaluation of atrial function and diseases. Minerva Cardioangiol. 58 (3), 379–397. http://www.ncbi.nlm.nih.gov/pubmed/20485242.

Guo, Rui, Zhong, Li, Ren, Jun, 2009. Overexpression of aldehyde dehydrogenase-2 attenuates chronic alcohol exposure-induced apoptosis, change in akt and pim signalling in liver. Clin. Exp. Pharmacol. Physiol. 36 (5–6), 463–468. http://dx.doi.org/10.1111/j.1440-1681.2009.05152.x.

Halpin, Laura E., Gunning, William T., Yamamoto, Bryan K., 2013. Methamphetamine causes acute hyperthermia-dependent liver damage. Pharmacol. Res. Perspect. 1 (1). http://dx.doi.org/10.1002/prp2.8.

He, Wei, Cheng, Zhi Huang, Yuan, Fang Li, Jian, Ping Xie, Rong, Ge Yang, Pei, Fu Zhou, Wang, Jian, 2008. One-step label-free optical genosensing system for sequence-specific dna related to the human immunodeficiency virus based on the measurements of light scattering signals of gold nanorods. Anal. Chem. 80 (22), 8424–8430. http://dx.doi.org/10.1021/ac801005d.

Hirsch, L.R., Stafford, R.J., Bankson, J.A., Sershen, S.R., Rivera, B., Price, R.E., Hazle, J.D., Halas, N.J., West, J.L., 2003. Nanoshell-mediated near-infrared thermal therapy of tumors under magnetic resonance guidance. Proc. Natl. Acad. Sci. U.S.A. 100 (23), 13549–13554. http://dx.doi.org/10.1073/pnas.2232479100.

Ibrahim, Khalid Elfaki, Bakhiet, Amel Omer, Awadalla, Maaweya Elaeed, Khan, Haseeb Ahmad, 2018. A priming dose protects against gold nanoparticles-induced proinflammatory cytokines mrna expression in mice. Nanomedicine 13 (3), 313–323. http://dx.doi.org/10.2217/nnm-2017-0332.

Ikegami, Aiko, Olsen, Christopher M., Fleming, Sheila M., Guerra, Erik E., Bittner, Michael A., Wagner, Jeremy, Duvauchelle, Christine L., 2002. Intravenous ethanol/cocaine self-administration initiates high intake of intravenous ethanol alone. Pharmacol. Biochem. Behav. 72 (4), 787–794. http://dx.doi.org/10.1016/S0091-3057(02)00738-4.

Ishak, Kamal, Baptista, Amelia, Bianchi, Leonardo, Callea, Francesco, De Groote, Jan, Gudat, Fred, Denk, Helmut, et al., 1995. Histological grading and staging of chronic hepatitis. J. Hepatol. 22 (6), 696–699. http://dx.doi.org/10.1016/0168-8278(95)80226-6.

Jackson, Lindsey N, Shawn D Larson, Scott R Silva, Piotr G Rychahou, L Andy Chen, Suimin Qiu, Srinivasan Rajaraman, et al. 2008. "PI3K/Akt Activation Is Critical for Early Hepatic Regeneration after Partial Hepatectomy" 536: 1401–10. https://doi.org/10.1152/ajpgi.00062.2008.

Jong, Wim H, De, Borm, Paul JA., 2008. Drug delivery and nanoparticles:applications and hazards. Int. J. Nanomed. 3 (2), 133–149. http://dx.doi.org/10.2147/IJN.S596.

Kang, N.J., Lee, K.M., Kim, J.H., Lee, B.K., Kwon, J.Y., Lee, K.W., Lee, H.J., 2008. Inhibition of gap junctional intercellular communication by the green tea polyphenol (-)-epigallocatechin gallate in normal rat liver epithelial cells. J Agric Food Chem 56 (21), 10422–10427. http://www.ncbi.nlm.nih.gov/entrez/query.fcgi?cmd=Retrieve&db=PubMed&dopt=Citation&list_uids=18828601.

Kedia, Satish, Sell, Marie A, Relyea, George, 2007. Mono- versus polydrug abuse patterns among publicly funded clients. Subst. Abuse Treat. Prev. Policy 2, 33. http://dx.doi.org/10.1186/1747-597X-2-33.

Khan, Haseeb A., Mohamed Anwar Abdelhalim, K., Al-Ayed, Mohammed S., Alhomida., Abdullah S., 2012. Effect of gold nanoparticles on glutathione and malondialdehyde levels in liver, lung and heart of rats. Saudi J. Biol. Sci. 19 (4), 461–464. http://dx.doi.org/10.1016/j.sjbs.2012.06.005.

Khan, Haseeb A., Mohamed Anwar Abdelhalim, K., Alhomida, Abdullah S., Al-Ayed, Mohammed S., 2013. Effects of naked gold nanoparticles on proinflammatory cytokines mRNA expression in rat liver and kidney. BioMed. Res. Int. 2013. http://dx.doi.org/10.1155/2013/590730.

Kirkpatrick, Matthew G., De Wit, Harriet, 2013. In the company of others: social factors alter acute alcohol effects. Psychopharmacology 230 (2), 215–226. http://dx.doi.org/10.1007/s00213-013-3147-0.

Koriem, Khaled M M, Soliman, Rowan E., 2014. Chlorogenic and caftaric acids in liver toxicity and oxidative stress induced by methamphetamine. J. Toxicol. 2014. http://dx.doi.org/10.1155/2014/583494.

Kurniawan, Alfin, Gunawan, Farrel, Nugraha, Adi Tama, Ismadji, Suryadi, Wang, Meng Jiy, 2017. Biocompatibility and drug release behavior of curcumin conjugated gold

nanoparticles from aminosilane-functionalized electrospun poly(N-Vinyl-2-Pyrrolidone) fibers. Int. J. Pharm. 516 (1–2), 158–169. http://dx.doi.org/10.1016/j.ijpharm.2016.10.067.

Kweon, Young-Oh, Paik, Yong-Han, Schnabl, Bernd, Qian, Ting, Lemasters, John J, Brenner, David A, 2003. Gliotoxin-mediated apoptosis of activated human hepatic stellate cells. J. Hepatol. 39 (1), 38–46. http://dx.doi.org/10.1016/S0168-8278(03)00178-8.

Loumaigne, Matthieu, Richard, Alain, Laverdant, Julien, Nutarelli, Daniele, Débarre, Anne, 2010. Ligand-induced anisotropy of the two-photon luminescence of spherical gold particles in solution unraveled at the single particle level. Nano Lett. 10 (8), 2817–2824. http://dx.doi.org/10.1021/nl100737y.

MacParland, Sonya A., Tsoi, Kim M., Ouyang, Ben, Ma, Xue Zhong, Manuel, Justin, Fawaz, Ali, Ostrowski, Mario A., et al., 2017. Phenotype determines nanoparticle uptake by human macrophages from liver and blood. ACS Nano 11 (3), 2428–2443. http://dx.doi.org/10.1021/acsnano.6b06245.

Mandal, Palash, Pritchard, Michele T., Nagy, Laura E., 2010. Anti-inflammatory pathways and alcoholic liver disease: role of an adiponectin/interleukin-10/heme oxygenase-1 Pathway. World J. Gastroenterol. 16 (11), 1330–1336. http://dx.doi.org/10.3748/wjg.v16.i11.1330.

Masserini, Massimo, 2013. Nanoparticles for brain drug delivery. ISRN Biochem. 2013, 1–18. http://dx.doi.org/10.1155/2013/238428.

Mironava, Tatsiana, Hadjiargyrou, Michael, Simon, Marcia, Jurukovski, Vladimir, Rafailovich, Miriam H, 2010. Gold nanoparticles cellular toxicity and recovery: effect of size, concentration and exposure time. Nanotoxicology 4 (1), 120–137. http://dx.doi.org/10.3109/17435390903471463.

Montet, Anne-Marie, Oliva, Laurence, Beaugé, Françoise, Montet, Jean-Claude, 2002. Bile salts modulate chronic ethanol-induced hepatotoxicity. Alcohol Alcohol. (Oxford, Oxfordshire) 37 (1), 25–29.

Nanji, Amin A., Mendenhall, Charles L., French, Samuel W., 1989. Beef fat prevents alcoholic liver disease in the rat. Alcohol.: Clin. Exp. Res. 13 (1), 15–19. http://dx.doi.org/10.1111/j.1530-0277.1989.tb00276.x.

Nieto, Natalia, 2006. Oxidative-stress and IL-6 mediate the fibrogenic effects of rodent kupffer cells on stellate cells. Hepatology 44 (6), 1487–1501. http://dx.doi.org/10.1002/hep.21427.

Noor, Neveen A, Heba M Fahmy, and Iman M Mourad. 2016. “Evaluation of the Potential Neurotoxicity of Gold Nanoparticles in the Different Rat Brain Regions” 4531 (December): 114–29.

Park, Ho Young, Choi, Hee Don, Eom, Hyojin, Choi, Inwook, 2013. Enzymatic modification enhances the protective activity of citrus flavonoids against alcohol-induced liver disease. Food Chem. 139 (1–4), 231–240. http://dx.doi.org/10.1016/j.foodchem.2013.01.044.

Pontes, Helena, Duarte, Jos Alberto, de Pinho, Paula Guedes, Soares, Maria Elisa, Fernandes, Eduarda, Dinis-Oliveira, Ricardo Jorge, Sousa, Carla, et al., 2008. Chronic exposure to ethanol exacerbates MDMA-induced hyperthermia and exposes liver to severe MDMA-induced toxicity in CD1 mice. Toxicology 252 (1–3), 64–71. http://dx.doi.org/10.1016/j.tox.2008.07.064.

Potter, James J., Mezey, Esteban, 2007. Acetaldehyde increases endogenous adiponectin and fibrogenesis in hepatic stellate cells but exogenous adiponectin inhibits fibrogenesis. Alcohol. Clin. Exp. Res. 31 (12), 2092–2100. http://dx.doi.org/10.1111/j.1530-0277.2007.00529.x.

Powell, Christine L., Bradford, Blair U., Craig, Christopher Patrick, Tsuchiya, Masato, Uehara, Takeki, O’Connell, Thomas M., Pogribny, Igor P., et al., 2010. Mechanism for prevention of alcohol-induced liver injury by dietary methyl donors. Toxicol. Sci. 115 (1), 131–139. http://dx.doi.org/10.1093/toxsci/kfq031.

Reif, Shimon, Lang, Alon, Lindquist, Jeffery N., Yata, Yutaka, Gäbele, Erwin, Scanga, Andrew, Brenner, David A., Rippe, Richard A., 2003. The role of focal adhesion kinase-phosphatidylinositol 3-kinase-Akt signaling in hepatic stellate cell proliferation and type I collagen expression. J. Biol. Chem. 278 (10), 8083–8090. http://dx.doi.org/10.1074/jbc.M212927200.

Sadauskas, Evaldas, Wallin, Håkan, Stoltenberg, Meredin, Vogel, Ulla, Doering, Peter, Larsen, Agnete, Danscher, Gorm, 2007. Kupffer cells are central in the removal of nanoparticles from the organism. Part Fibre Toxicol. 4 (3), 10. http://dx.doi.org/10.1186/1743-8977-4-10.

Safieh-Garabedian, B., Poole, S., Allchorne, A., Winter, J., Woolf, C.J., 1995. Contribution of interleukin-1 beta to the inflammation-induced increase in nerve growth factor levels and inflammatory hyperalgesia. Br. J. Pharmacol. 115 (7), 1265–1275. https://doi.org/0007-1188/95.

Sayette, Michael A., Creswell, Kasey G., Dimoff, John D., Fairbairn, Catharine E., Cohn, Jeffrey F., Heckman, Bryan W., Kirchner, Thomas R., Levine, John M., Moreland, Richard L., 2012. Alcohol and group formation: a multimodal investigation of the effects of alcohol on emotion and social bonding. Psychol. Sci. 23 (8), 869–878. http://dx.doi.org/10.1177/0956797611435134.

Schaeublin, Nicole M, Braydich-Stolle, Laura K, Schrand, Amanda M, Miller, John M, Hutchison, Jim, Schlager, John J, Hussain, Saber M, 2011. Surface charge of gold nanoparticles mediates mechanism of toxicity. Nanoscale 3, 410–420. http://dx.doi.org/10.1039/c0nr00478b.

Seki, Ekihiro, De Minicis, Samuele, Osterreicher, Christoph H, Kluwe, Johannes, Osawa, Yosuke, Brenner, David A., Schwabe, Robert F., 2007. TLR4 enhances TGF-beta signaling and hepatic fibrosis. Nat. Med. 13 (11), 1324–1332. http://dx.doi.org/10.1038/nm1663.

Sereemaspun, Amornpun, Rojanathanes, Rojrit, Wiwanitkit, Viroj, 2008. Effect of gold nanoparticle on renal cell: an implication for exposure risk. Ren. Fail. 30 (3), 323–325. http://dx.doi.org/10.1080/08860220701860914.

Son, Yong, Cheong, Yong-Kwan, Kim, Nam-Ho, Chung, Hun-Taeg, Kang, Dae Gill, Pae, Hyun-Ock, 2011. Mitogen-activated protein kinases and reactive oxygen species: how can ROS activate MAPK pathways? J. Signal Trans. 2011, 792639. http://dx.doi.org/10.1155/2011/792639.

Sumbayev, Vadim V., Yasinska, Inna M., Garcia, Cesar Pascual, Gilliland, Douglas, Lall, Gurprit S., Gibbs, Bernhard F., Bonsall, David R., Varani, Luca, Rossi, François, Calzolai, Luigi, 2013. Gold nanoparticles downregulate interleukin-1β-induced pro-inflammatory responses. Small 9 (3), 472–477. http://dx.doi.org/10.1002/smll.201201528.

Tang, Yuhan, Li, Yanyan, Haiyan, Yu., Gao, Chao, Liu, Liang, Xing, Mingyou, Liu, Liegang, Yao, Ping, 2014. Quercetin attenuates chronic ethanol hepatotoxicity: implication of ‘free’ iron uptake and release. Food Chem. Toxicol. 67, 131–138. http://dx.doi.org/10.1016/j.fct.2014.02.022.

Tilg, Herbert, Moschen, Alexander R., 2008. Inflammatory mechanisms in the regulation of insulin resistance. Mol. Med. (Cambridge, Mass.) 14 (3–4), 222–231. http://dx.doi.org/10.2119/2007-00119.Tilg.

Tokunaga, Itsuo, Kubo, Shin-ichi, Ishigami, Akiko, Gotohda, Takako, Kitamura, Osamu, 2006. Changes in renal function and oxidative damage in methamphetamine-treated rat. Legal Med. (Tokyo, Japan) 8 (1), 16–21. http://dx.doi.org/10.1016/j.legalmed.2005.07.003.

Tsai, Chiau-Yuang, Shiou-Ling Lu, Chia-Wen Hu, Chen-Sheng Yeh, Gwo-Bin Lee, and Huan-Yao Lei. 2012. “Size-Dependent Attenuation of TLR9 Signaling by Gold Nanoparticles in Macrophages.” Journal of Immunology (Baltimore, Md. : 1950) 188 (1): 68–76. https://doi.org/10.4049/jimmunol.1100344.

Wang, Jun Ying, Chen, Jie, Yang, Jiang, Wang, Hao, Shen, Xiu, Sun, Yuan Ming, Guo, Meili, Zhang, Xiao Dong, 2016. Effects of surface charges of gold nanoclusters on long-term in vivo biodistribution, toxicity, and cancer radiation therapy. Int. J. Nanomed. 11, 3475–3485. http://dx.doi.org/10.2147/IJN.S106073.

Wells, Peter G., Shama Bhatia, Danielle M. Drake, and Lutfiya Miller-Pinsler. 2016. “Fetal Oxidative Stress Mechanisms of Neurodevelopmental Deficits and Exacerbation by Ethanol and Methamphetamine.” Birth Defects Research Part C - Embryo Today: Reviews. https://doi.org/10.1002/bdrc.21134.

Wen, Donghai, Huang, Xinzhong, Zhang, Min, Zhang, Liying, Chen, Jing, Yong, Gu., Hao, Chuan Ming, 2013. Resveratrol attenuates diabetic nephropathy via modulating angiogenesis. PLoS One 8 (12). http://dx.doi.org/10.1371/journal.pone.0082336.

Winkler, Madeline C., Greager, Emilee M., Stafford, Jacob, Bachtell, Ryan K., 2016. Methamphetamine self-administration reduces alcohol consumption and preference in alcohol-preferring P rats. Addict. Biol. http://dx.doi.org/10.1111/adb.12476.

Yang, Raymond S H, Chang, Louis W., Jui Pin, Wu., Tsai, Ming Hsien, Wang, Hsiu Jen, Kuo, Yu Chun, Yeh, Teng Kuang, Yang, Chung Shi, Lin, Pinpin, 2007. Persistent tissue kinetics and redistribution of nanoparticles, quantum dot 705, in mice: ICP-MS quantitative assessment. Environ. Health Perspect. 115 (9), 1339–1343. http://dx.doi.org/10.1289/ehp.10290.

Yue, Min, Ni, Qun, Chao Hui, Yu., Ren, Ke Ming, Chen, Wei Xing, Li, You Ming, 2006. Transient elevation of hepatic enzymes in volunteers after intake of alcohol. Hepatobiliary Pancreatic Dis. Int. 5 (1), 52–55.

Zendulka, O., Sabová, M., Juřica, J., MacHalíček, M., Švéda, P., Farková, M., Šulcová, A., 2012. The effect of methamphetamine on biotransformation of ethanol: pilot study. Acta Facultatis Pharm. Univ. Comenianae 59 (2), 63–71. http://dx.doi.org/10.2478/v10219-012-0026-4.

Zhang, Qin, Hitchins, Victoria M, Schrand, Amanda M, Hussain, Saber M, Goering, Peter L, 2011. Uptake of gold nanoparticles in murine macrophage cells without cytotoxicity or production of pro-inflammatory mediators. Nanotoxicology 5 (September), 284–295. http://dx.doi.org/10.3109/17435390.2010.512401.

Zhang, Xiao Dong, Hong Ying, Wu., Di, Wu., Wang, Yue Ying, Chang, Jian Hui, Zhai, Zhi Bin, Meng, Ai Min, Liu, Pei Xun, Zhang, Liang An, Fan, Fei Yue, 2010. Toxicologic effects of gold nanoparticles in vivo by different administration routes. Int. J. Nanomed. 5 (1), 771–781. http://dx.doi.org/10.2147/IJN.S8428.

Zhang, Juan, Tang, Hongju, Zhang, Yuqing, Deng, Ruyuan, Shao, Li, Liu, Yun, Li, Fengying, Wang, Xiao, Zhou, Libin, 2014. Identification of suitable reference genes for quantitative RT-PCR during 3T3-L1 adipocyte differentiation. Int. J. Mol. Med. 33 (5), 1209–1218. http://dx.doi.org/10.3892/ijmm.2014.1695.